



Universidade de Aveiro Departamento de Química
2019

Maria Carlos Oliveira

Impressão 3D de *scaffolds* com dupla porosidade para modular a resposta imune

Dual porosity 3D printed scaffolds to modulate the immune response



Universidade de Aveiro Departamento de Química
2019

Maria Carlos Oliveira

Impressão 3D de *scaffolds* com dupla porosidade para modular a resposta imune

Dual porosity 3D printed scaffolds to modulate the immune response

Dissertação apresentada à Universidade de Aveiro para cumprimento dos requisitos necessários à obtenção do grau de Mestre em Bioquímica, com especialização em Bioquímica Clínica, realizada sob a orientação científica da Doutora Sandra Camarero-Espinosa, Investigadora Pós-Doutorada do MERLN Institute for Technology-Inspired Regenerative Medicine, do Professor Doutor Lorenzo Moroni do MERLN Institute for Technology-Inspired Regenerative Medicine e do Professor Doutor João Mano, Professor Catedrático do Departamento de Química da Universidade de Aveiro.

o júri

Presidente

Professor Doutor Lorenzo Moroni

Professor da Universidade de Maastricht e Coordenador do departamento Complex Tissue Regeneration no MERLN Institute for Technology-Inspired Regenerative Medicine

Vogal -Arguente Principal

Doutora Niloofar Tahmasebi Birgani

Investigadora Pós-Doutorada do departamento Instructive Biomaterials Engineering (IBE) no MERLN Institute for Technology-Inspired Regenerative Medicine

Vogal - Orientador

Doutora Sandra Camarero-Espinosa

Investigadora Pós-Doutorada do departamento Complex Tissue Regeneration (CTR) no MERLN Institute for Technology-Inspired Regenerative Medicine

Agradecimientos

In the end of this journey, I know that I wouldn't do this master thesis alone and because of that I would like to acknowledge all the people that support and assist me.

To Dr. Sandra Camarero-Espinosa, my mentor on this project that supported me scientifically and motivated me to aspire the best inside me, every day, having in her an inspiration.

To Prof. Lorenzo Moroni for allowing me to learn in his lab and to be part on all the essential discussions in this project.

To Prof. João Mano to recommended me MERLN to follow my master thesis, for all the support and to ease the contact with my university.

To Andrea Calore for the great micro-CT images acquisition and Víctor Galván for the profilometer analysis. Carlotta Mondadori for all the discussions about these strong cells, macrophages. Claire Polain for the help with support bath and to be my partner on 3D-TIPS scaffolds fabrication.

To the whole MERLN and more specifically CTR department, where I learned a lot not only about regenerative medicine but about science in general. To all the people in the labs or in the office that asked me challenging questions or gave me answers every time that I needed help, such as Clarissa, Tobias, Ravi, Kenny and Shahzad.

To all my friends in Portugal that never forget me while I was far away. To the friends I gained here in Maastricht that helped me overcome the down moments and cheer for the good ones: João, Marta, Mónica, Daniel, Filipa, Rosa, Sara, Cathrin, Núria and Annabe.

To Francisco for being with me in all moments, believing in me every time I could not and to give me energy for being a better person and a better scientist.

To my family and specially my parents to always give me a place where I can come back safely and to believing in me in all my adventures making me smile every day.

“Apart from that, I have in me all the dreams in the world.”

Palavras Chave: Manufatura Aditiva; TIPS; Macrófagos; Resposta Imune;

Resumo

Além do conhecimento avançado sobre a fabricação de biomateriais complexos, a modulação da resposta do hospedeiro ainda é um desafio em aplicações médicas. Os principais reguladores dessa resposta são os macrófagos que podem polarizar de um fenótipo pró-inflamatório (M1) para um fenótipo anti-inflamatório (M2) e afetar a resposta imune. Atualmente, estratégias para influenciar a ativação de macrófagos para a medicina regenerativa são exploradas para melhor entender o seu papel complexo. Idealmente, esta modulação seria conseguida alterando as propriedades físico-químicas (por exemplo, rigidez, porosidade, topografia) de um biomaterial sem a adição de citocinas exógenas, fatores de crescimento ou terapias celulares complicadas. Assim, este trabalho teve como objetivo criar *scaffolds* impressos em 3D com porosidade dupla e topografia controlável, que podem ajustar a resposta de corpos estranhos, fabricados a partir de manufatura aditiva e TIPS (Separação de Fases Termicamente Induzida). Dois polímeros de poli(ϵ -caprolactona-co-lactida) (PCLLA) com diferentes cristalinidades foram utilizados para fabricar os *scaffolds* e apresentaram maior porosidade e rugosidade superficial do que os *scaffolds* de FDM (Modelagem por Deposição Fundida). Os *scaffolds* 3D-TIPS, mais ásperos e porosos, apresentaram maior adesão celular e diminuição da citocina pró-inflamatória, TNF- α , em comparação aos *scaffolds* de FDM. A partir dos resultados in vivo, *scaffolds* da composição amorfa de PCLLA mostraram maior degradação do que a mais cristalina, resultando em cápsula fibrosa mais densa a cobrir o biomaterial. Os *scaffolds* 3D-TIPS também mostraram mais infiltração celular dentro das fibras, sugerindo poros interconectados, mas os *scaffolds* de FDM mostraram grande capacidade de infiltração celular pela sua porosidade no eixo z no polímero mais cristalino.

Por fim, os dados indicam um grande potencial para os *scaffolds* 3D-TIPS para suprimir o fenótipo pró-inflamatório comparando com a técnica FDM, pelo aumento da rugosidade e porosidade.

Keywords:

Additive Manufacturing; TIPS; Macrophages; Immune Response;

Abstract

Besides the advanced knowledge on the fabrication of complex implant biomaterials, modulating the host response is still an unmet challenge in medical applications. The main regulators of this response are the macrophages that can polarize from a pro-inflammatory (M1) phenotype to an anti-inflammatory phenotype (M2) and affect the path of the immune response. Nowadays, strategies to influence macrophage activation for regenerative medicine are being explored to better understand their complex role. Ideally, this modulation would be achieved by altering the physicochemical properties (e.g. stiffness, porosity, topography) of a biomaterial without the addition of exogenous cytokines, growth factors or complicated cell therapies. Thus, this work aimed to create 3D-printed scaffolds with dual porosity and controllable topography, that can tune the foreign body response, fabricated from additive manufacturing and Thermally Inducible Phase Separation (TIPS). Two polymers of Poly(ϵ -caprolactone-co-lactide) (PCLLA) with different crystallinity were used to fabricate the scaffolds and showed higher porosity and surface roughness than Fused Modelling Deposition (FDM) scaffolds. 3D-TIPS scaffolds, that were rougher and more porous, showed higher cell adhesion and decrease of pro-inflammatory cytokine, TNF- α , comparing to FDM scaffolds. From the *in vivo* results, scaffolds from the amorphous PCLLA composition showed greater degradation than the more crystalline one, resulting in denser fibrous capsule around the biomaterial. 3D-TIPS scaffolds also showed more cell infiltration inside the fibers suggesting interconnected pores, but FDM scaffolds showed great capacity for cell infiltration by its porosity on the z-axis on the more crystalline polymer. Together, these data indicate a great potential for 3D-TIPS scaffolds to suppress pro-inflammatory phenotype comparing with FDM, by increased roughness and porosity.

Contents

1. Introduction	1
1.1. Modulation of Immune Response	1
1.1.1. Stiffness	3
1.1.2. Structure	4
1.1.3. Porosity	4
1.1.4. Surface Topography	5
2. Porous Scaffold Fabrication	6
2. Materials and Methods	8
2.1. Materials	8
2.2. Scaffold Fabrication	8
2.3. Scaffold Characterization	8
2.4. Support Bath	9
2.5. Cell Culture	9
2.6. Cell culture on spin-coated polymer films	10
2.7. 3D Cell Culture	10
2.8. Macrophage polarization	10
2.9. Live/Dead	10
2.10. Lactase dehydrogenase (LDH) Assay	10
2.11. Quantification of DNA	11
2.12. Immunofluorescence	11
2.13. SEM of cell cultures on scaffolds	11
2.14. Cytokine secretion	12
2.15. <i>In vivo</i> Experiments	12
2.16. Statistical Analysis	12
3. Results and Discussion	13
3.1. Fabrication of PCLLA 3D-TIPS scaffolds	13
3.2. <i>In vitro</i> cellular response to PCLLA polymer films	18
3.3. <i>In vitro</i> cellular response to PCLLA scaffolds	23
3.4. M2 macrophage influence on mesenchymal stem cells (MSCs)	26
3.5. Support Bath	28

3.6. <i>In vivo</i> response to PCLLA scaffolds.....	30
4. Conclusion.....	33
5. Valorisation	35
6. References	36
Supplemental Information	40

List of Figures

Figure 1 - Foreign Body Reaction after biomaterial implantation. Adapted from (4)	2
Figure 2 - Schematic temperature–composition phase diagram of a binary polymer solution. Adapted from (47)	7
Figure 3 – SEM images of the 3D TIPS scaffolds. Axial view of the A) 7% PCLLA PG with 87%/13% ratio of 1,4 dioxane/water; B) 7% PCLLA PG with 90%/10% ratio of 1,4 dioxane/water; C) 7% PCLLA CB7015 with 87%/13% ratio of 1,4 dioxane/water; D) 5% PCLLA PG; E) 7% PCLLA PG; F) 9% PCLLA PG. Fibers inset in A1 and B1, and cross-sectional views in the upper corners of C, D, E, F. A1-C1 scale= 200μm, C1-F1=500μm, C2-F2 scale =50 μm	14
Figure 4 - Representative images of μ-CT analysis of A) 5% PG, B) 7%PG, C) 5% PG and D) 7% PG.	15
Figure 5 - Representative images of the scaffolds from the axial and cross section with A) 5%CB, B) 7% CB, D) 5% PG and E) 7%PG and the FDM scaffolds from CB (C) , and PG (F). The images of fiber geometry are in upper corner of A1-F1, scale=200μm and the porosity inside the fibers of A2-F2, scale=50μm.	16
Figure 6 - Wettability (A) and physical properties of all the scaffolds. B) indicates the data from GPC analysis, C) Surface Roughness, D) Representative images of surface roughness where Left up: CB7, Right up: CB100. Left down: PG 7 and right down: CB100.	17
Figure 7 - Biochemical assays for assessment of cell viability by the materials (A, C), cytotoxicity (B) and cell attachment by the DNA assay (D), Scale bar= 100μm.	19
Figure 8 – Immunofluorescence images with staining of F-actin (red), Paxilin (green) and cell nuclei (blue) for PG (A), CB (B) and TCP, Scale bar=50μm.....	20
Figure 9 – TNF-α expression of macrophages in response to polymer films (P for PG and C for CB) or TCP (K) with 10 ng / mL LPS/IFN- γ (M1), 20 ng / mL IL-4/IL-13 (M2) or unstimulated (0).	21
Figure 10 – IF and brightfield images of macrophages in response to TCP culture and 10 ng / mL LPS/IFN-γ (M1), 20 ng / mL IL-4/IL-13 (M2) or unstimulated (M0). Nuclei (blue), Arginase-1 (Green) iNOS (red) are represented. Scale bar=200μm	22
Figure 11 - IF and brightfield images of macrophages in response to CB culture and 10 ng / mL LPS/IFN-γ (M1), 20 ng / mL IL-4/IL-13 (M2) or unstimulated (M0). Nuclei (blue), Arginase-1 (Green) iNOS (red) are represented. Scale bar=200μm	22
Figure 12 - IF and brightfield images of macrophages in response to PG culture and 10 ng / mL LPS/IFN- γ (M1), 20 ng / mL IL-4/IL-13 (M2) or unstimulated (M0). Nuclei (blue), Arginase-1 (Green) iNOS (red) are represented. Scale bar=200μm	23
Figure 13 – Immunofluorescence images stained for F-actin of the cells seeded on scaffolds. Scale bar: 1mm.	24

Figure 14 – SEM images representing the changes of macrophage morphology on the different scaffolds. Scale bar: 20µm.....	25
Figure 15 – IF images of macrophages seed on CB7, CB100 and PG7 scaffolds. The PG100 condition is not shown because of low cell attachment. Scale bar=50µm	26
Figure 16 – A: DNA content and B: TNF- α cytokine secretion by macrophages adhered to the scaffolds after 3 days of culture.....	26
Figure 17 – IF images stained for F-actin (red) and Nuclei (blue) with different scaffolds. Here the H, stands out for basal media hMSCs conditions and M for hMSCS treated with M2-stimulated macrophages secretome Scale=100µm and in upper corner scale= 1mm. .	28
Figure 18 – Photographs for Lecithin gels in the right of the panel and Gelatine in the left.	29
Figure 19 - Cellular infiltration and matrix deposition in scaffolds produced by 3D-TIPS and FDM after subcutaneous implantation for 3 weeks (1) and 6 weeks (2): (Left) tissue integration by Hematoxylin and Eosin (H&E) staining and (Right) collagen production by Masson's trichrome (M&T) staining. A) CB7, B) CB100, C) PG7 and D) PG100 are represented in low magnification (scale = 2000µm) and a x4 magnification (scale = 500µm) in the upper corner.	32

Abbreviations

BSA Bovine serum albumine

CB Poly (70/30) L Lactide ϵ Caprolactone

ChD/ChO Chitosan scaffolds with diagonal/orthogonal geometry

DMF Dimethylformamide

ECM Extracellular Matrix

FBGC Foreign Body Giant Cell

FBR Foreign Body Reaction

FDM Fused deposition modelling

GPC Gel permeation chromatography

IFN- γ Interferon gamma

IL-4 Interleukin-4

IL-13 Interleukin -13

LDH Lactate dehydrogenase

LPS Lipopolysaccharide

MCP-1 Monocyte Chemoattractant Protein-1

micro-CT X-Ray micro computed tomography

MSC Mesenchymal stem cells

PCL Polycaprolactone

PCLLA Poly(ϵ -caprolactone-co-lactide)

PG (Poly (68/32[15/85 D/L]) Lactide ϵ Caprolactone

PLA Polylactide

ROS Reactive Oxygen Species

SEM Scanning Electron Microscopy

TCP Tissue culture plate

THP-1 Monocytic human cell line from acute monocytic leukemia

TIPS Thermally Inducible Phase Separation

TNF- α Tumor necrosis factor- α

VEGF Vascular Endothelial Growth factor

WCA Water contact angle

1. Introduction

1.1. Modulation of Immune Response

Tissue engineering and regenerative medicine are increasingly wide fields focused on the in-vitro fabrication or in-vivo formation of neo-tissues capable of replacing the damaged ones. To this end, biomaterial scaffolds capable of directing the formation of coherent tissues are designed, fabricated and ultimately implanted on the body. Besides the progression of the knowledge on the fabrication of complex implant biomaterials, the immune response that all implantation procedures face is still a challenge in medical application. The implantation is followed by a sequence of events termed foreign body reaction (FBR), represented in Fig. 1. The FBR can lead to the encapsulation of the biomaterial by collagen fibers, restraining the interaction between the tissue and the implant since the cell migration and transportation of oxygen and nutrients is stopped, and ultimately lead to a complete failure of the implant (1).

Upon implantation, inflammation of the area occurs. The process of inflammation starts when plasma components and extracellular matrix (ECM) proteins are adsorbed to the biomaterial through hydrophobic, charge interactions, or through protein conformational changes (2). These include albumin, fibrinogen, vitronectin, fibronectin and complement factors, and the attachment of these proteins can affect the inflammatory response to biomaterials (3). Simultaneously to the protein adsorption, the activation of the coagulation cascade also occurs, leading to the formation of a provisional matrix, fibrin predominant, capable of recruiting immune cells (lymphocytes, neutrophils and monocytes or macrophages) by the production of growth factors, cytokines and chemoattractants (4,5).

The protein layer offers binding sites to neutrophils, monocytes and macrophages by their protein specific receptors, like integrins or pattern recognition receptors (1,5). The neutrophils not only promote the destruction of pathogens by secretion of proteolytic enzymes and reactive oxygen species (ROS) but also have a regulatory function by secretion of chemokines that will activate monocytes, macrophages, dendritic cells and lymphocytes. The continuous release of chemokines like interleukin-8 (IL-8), monocyte chemoattractant protein-1 (MCP-1) and macrophage inflammatory protein-1 β (MIP-1 β) suppresses neutrophils infiltration and these cells disappear from the implantation site by macrophages phagocytosis (1).

The circulating monocytes migrate to the implantation and differentiate to M1 phenotype, also called “classically activated”. The adhesion occurs by the interaction between β 2 integrins of monocytes and the adsorbed proteins (1,4). From that, the M1 macrophages secrete not only pro-inflammatory cytokines, such as tumour necrosis factor- α (TNF- α), IL-1, IL-6, and IL-8, but also ROS and nitrogen species for antimicrobial and phagocytic activity (1,4). In the latter stage of the FBR, macrophages can fuse to a Foreign Body Giant Cell (FBGC) and polarize to M2 phenotype with pro-healing capacities. The FBGC is formed to increase the phagocytic ability and it is promoted by the interaction

between $\beta 1$ integrins from macrophages and vitronectin adsorbed in the biomaterial (6,7). It has been shown that the main inducers of macrophage fusion are the cytokines IL-4 and IL-13 (8,9). The FBGC secretes anti-inflammatory cytokines (IL-10 and IL-1ra), ROS and degradative enzymes around the biomaterial (1) and, the increased secretion of the latter substances makes FBGC detrimental not only to the biomaterial but also to the surrounding tissue (4). Besides FBGC, IL-4 and IL-13 also polarize macrophages to an M2 phenotype. The M2 phenotype has been indicated as a pro-regenerative phenotype because of the stimulation of fibroblasts to remodel the tissue and the increasing vascularization. However, the chronic stimulation of this phenotype leads to the formation of a fibrous capsule at the end of the FBR (10,11).

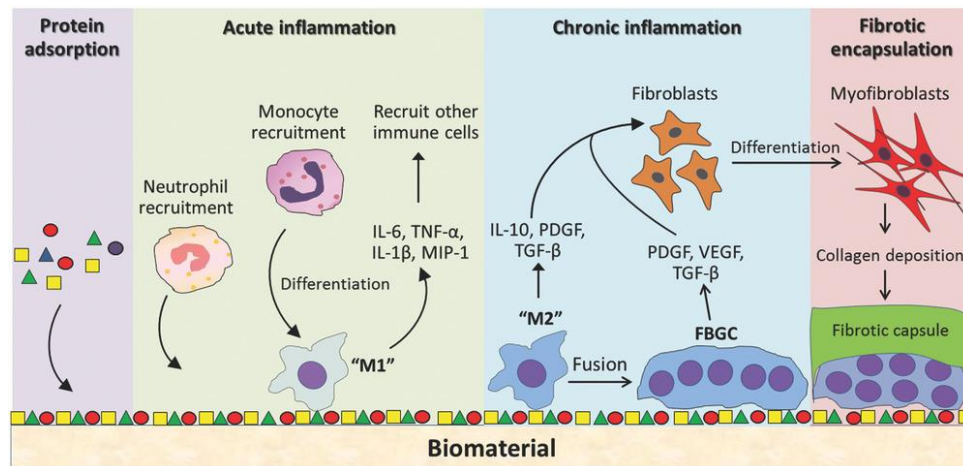


Figure 1 - Foreign Body Reaction after biomaterial implantation. Adapted from (4)

The fibrous capsule is formed by the activation of fibroblasts which is induced by TGF- β , platelet-derived growth factor (PDGF) and vascular endothelial growth factor (VEGF) secreted by macrophages and by FBGC. Fibroblasts will then differentiate into myofibroblasts that activate the production of collagen fibers (1,12). In a normal wound healing, the fibroblasts and myofibroblasts go to apoptosis and senescence, and the collagen levels decrease (13). However, this does not occur in FBR mostly because of the continuous stimulation of pro-inflammatory and pro-fibrotic cells around the biomaterial, leading to an excessive fibrosis (4,12). For this reason, numerous approaches have been applied to biomaterials to alter the fate of the immune response.

The study on macrophages has gained attention in tissue engineering field since they can polarize to different phenotypes modelling their function and thus, the progress of FBR leading to a pro-inflammatory or pro-healing environment. The phenotypic response is usually simplified in a M1 and M2 dichotomy and it is studied by alterations in gene expression, inducing stimuli, metabolism, surface markers and its functions (10). This was first introduced because the T-helper (Th) Cells, Th1 and Th2, activate macrophages to a pro-inflammatory response, M1 phenotype, and to anti-inflammatory, M2 phenotype, respectively (14). However, the knowledge of the mechanisms behind the polarization of

macrophages has increased and the M2 have been divided onto many different subtypes. The M2a subtype is stimulated by IL-4 and IL-13, M2b is stimulated by immunocomplexes and toll-like receptor (TLR) agonists, like lipopolysaccharide (LPS), and M2c is induced by IL-10. M2a and M2c seem to have great importance in pro-regenerative response since they secrete IL-10, IL-1ra and transforming growth factor- β (TGF- β) (10,15). The complexity of the polarization of macrophages and the inconsistency of the used sub-types of M2 in experiments led to a proposal to change the nomenclature to describe each type by its activator, for instance M (LPS) (16). However, the M1-M2 dichotomy is still broadly used since it simplifies and makes macrophage biology comprehensible for *in vitro* experiments (17), even being an oversimplification for the full spectrum of phenotypes that occur *in vivo* (18).

The implantation of biomaterials, recently, has shifted from an immunosuppressive to a comprehensive approach of the immune system. Different strategies have been applied to modulate the immune system, such as: a) altering the chemical properties of the biomaterial; b) controlling the release of bioactive factors; c) cell therapy methods; and d) changing the physical properties of the biomaterial (19). Ideally, this modulation would be achieved by altering the physicochemical properties of a biomaterial without the addition of exogenous cytokines or growth factors or complicated cell therapies.

The physical properties of the biomaterial are sensed by macrophages and interfere with their shape. Depending on the substrate, macrophages can be rounded or with uniaxial and biaxial stretches and these changes affect migration of macrophages (20). Cell shape have been shown to affect polarization of macrophages, for instance elongated cell in murine macrophages induced M2 phenotype (21). However, this relationship is still unclear since it is also affected by cell line used and by others bioactive factors in the microenvironment.

1.1.1. Stiffness

It has been shown that substrate stiffness of biomaterials can affect cell migration, proliferation, spread area and cytokine secretion (22–24). Cell culture of human monocyte-derived macrophages in polyacrylamide gels with various stiffness revealed that stiffer gels (280kPa) promoted higher proliferation rate than their softer counterparts (1-5kPa) (24). Phagocytosis by the murine cell line Raw 264.7 (derived from Abelson murine leukemia virus-induced tumor) and by the human derived macrophages, alveolar macrophages and THP-1 (monocytic human cell line from acute monocytic leukemia) derived was evaluated by the number of internalized beads. The results show an increase in gels with 150kPa and 88kPa compared to softer substrates (22,23). However, Sridharan et al., proposed that there is a range limit where the phagocytic capacity is impaired. They showed that the highest phagocytic activity was in 88kPa gel, the intermediate level of stiffness, but the stiffest gel (323kPa) and plastic plate had lower phagocytic activity. (23). The impact of stiffness in phagocytosis could be related to actin organization and migration modes. It was reported that macrophages have the ability to change their migration mode from a faster, amoeboid migration, to a slow, mesenchymal migration, depending on their morphology (25). The

mesenchymal migration is indicated as having more protrusions as opposed to the amoeboid migration that represents rounded cells (25). In comparison to macrophages in softer gels, the ones in the stiffer gels are more elongated and present filopodia protrusions (22–24,26,27) and substrate stiffness alone seemed to be a factor to modulate macrophages to a mesenchymal migration (23).

The secretion of cytokines is also affected by substrate stiffness but it is still unclear which phenotype is induced. Some studies showed increased values of pro-inflammatory cytokines, such as TNF- α , IL-1 β or IL-6 when culturing murine primary bone marrow-derived macrophages (BMM) and THP-1 derived macrophages cells in stiff gels (230kPa (26), 323kPa (23).and 840kPa (27)), upon LPS stimulation. Without LPS stimulation, Previtera et. al showed changes in the levels of pro-inflammatory cytokines with stiffness alone, however in a separate study, it was shown that BMM were unresponsive to stiffness itself (26,27). This contradictory data makes the effect of stiffness in cytokine secretion by macrophages still questionable. The differences could be related to the substrate stiffness range or by the different type of material used, suggesting that the chemical properties of the material also play a significant role in macrophage polarization. Even with this question in mind, stiffness has shown differences on suppression of the pro-inflammatory effect of LPS, showing the softest materials the highest suppression pro-inflammatory phenotype suppression levels (27). Moreover, Gruber et al. showed that in stiffer gels, BMM express higher levels of TNF- α (28). But with Raw 264.7 cells, the TNF- α secretion was lower in medium stiffness materials (20kPa) and no significant differences between soft (1kPa) and stiff gel was found (28). The differences between cell lines suggest that changing cell types can alter the stiffness sensibility and that there is a need to take these parameters in consideration.

1.1.2. Structure

The morphology of biomaterials such as fibrillar, spherical or porous, have been studied as a parameter for the modulation of macrophage polarization. For instance, spheres larger than 1.5mm suppressed the FBR and fibrosis for a long period in different materials: alginate, hydrogel, metals, glass and plastic (29). Fibrillar structures have also been reported to impact macrophages since these mimic the ECM. The role of parameters such as fiber diameter and alignment have been studied and compared in terms of activation, morphology and cytokine secretion of macrophages(30–32). In a study, with the application of vascular grafts, PCL electrospun scaffolds were tested *in vitro* and *in vivo* for the immune response of macrophages. The grafts with thicker fibers (~6 μ m) had higher porosity and expressed more anti-inflammatory cytokines than the thinner-fiber grafts (0.7 μ m) in RAW 264.7 macrophages (30).

1.1.3. Porosity

Similar to the structure, the porosity is also a determinant factor in foreign body reaction. It was shown that the size and organization of pores affects fibrosis, vascularization

and macrophage polarization (33). Almeida et al., showed that, besides the material chemistry itself (PLA and Chitosan) the pore geometry also impacted the cytokine secretion over time (3,7 and 10 days) and morphology of macrophages. Chitosan scaffolds with orthogonal i.e 90° (ChO) and diagonal i.e 45° (ChD) geometries were fabricated using rapid prototyping and rounder macrophages were found in the former, while more elongated cells were found in the latter. Moreover, in ChO scaffolds higher levels of secreted TNF- α and IL-12/23 were detected, especially in late time points, than in ChD scaffolds while IL-10 remained low in both scaffolds. A higher metabolic activity and cytokine secretion was measured in ChO scaffolds, suggesting that ChO with larger pores induce a stronger inflammation (33).

The effect of porosity has also been shown to reduce fibrosis while inducing vascularization (34). In an *in-vivo* study, sphere-templated poly (2-hydroxyethyl methacrylate) scaffolds with various pore sizes were implanted, for 3 weeks, in BAT-gal mice. The scaffolds with 34 μ m interconnected pore structure showed a thinner and less dense fibrous capsule and higher cell infiltrate, than its non-porous counterpart. When the same material presented 160 μ m pores, a thicker fibrous capsule was formed after 3 weeks of implantation than with 34 μ m pores but not greater as the non-porous material. The smallest pores (34 μ m) showed also increased blood vessel density. This *in vivo* study also suggested that macrophage polarization had an impact in fibrosis, showing higher values of M2 markers in the fibrous capsule (34). The results not only showed that porosity has an impact in the FBR but, also, that depending on the size of the pores the macrophage polarization and thus, the FBR formation differ.

1.1.4. Surface Topography

Surface topography modulates the activity of local macrophages by altering their shape. Macrophages tend to elongate when cultured on 400-500 nm width grooves and, secrete higher amounts of anti-inflammatory cytokines (21,35–37). This shows that not only biological factors polarize macrophages onto a specific phenotype but, the mechanobiology behind it is also an important aspect. McWhorter and Wang showed that cell elongation leads towards a M2 phenotype by increased expression of arginase-1 and CD206 (macrophage mannose receptor) (21). Although these cytokine release values were not as high as when cells were stimulated with IL-4/IL-13 cytokines, the cytoskeletal arrangement that leads to elongated cells also seemed to decrease the expression of proinflammatory cytokines (21).

The effect in macrophage elongation with grooves of different widths was tested using parallel grooves by Chen (36) (0.25 μ m to 2 mm line widths) to Raw 264.7 cells and by Luu (37) (0.15 to 50 μ m width) to BMM cells. The first study showed that the effects were independent on the material used (PCL, PLA or PDMS) but, with different groove sizes, the macrophages change their shape and cytokine expression over the time. The macrophage elongation increased with decreasing topography until 500nm since cells showed insensitivity at 250nm, after 48h. They also showed that the cytokine expression change over time in the early inflammation (6h, 24h, 48h), suggesting a transition from pro-

inflammatory (TNF- α , MIP-1 α , MCP-1) at 6h and 24h to pro-healing cytokines at 48h (VEGF). According to *in vivo* studies, by subcutaneous implantation on Sprague–Dawley rats, no differences in cell elongation were observed at day 7 and 21 after implantation (36). In the second study similar results were presented, showing that the highest degree of elongation appeared when cells were cultured on surfaces with 450-500nm grooves. Moreover, the expression of Arginase-1 was higher on grooves of widths from 400nm to 5 μ m. In addition, IL-10 secretion was more intense in 5 μ m width grooves, whereas the TNF- α secretion remained low in all conditions (37). Altogether, this data shows that there is a limit in groove size where macrophages elongate and express M2 markers but, besides their shape alteration, the expression of M1 markers were not affected. In summary, grooves with sizes ranging from 400 nm to 5 μ m seem to be associated with a pro-healing phenotype.

Unidirectional gratings are shown as the greater stimulators of elongation in contrast with bidirectional gratings. In 1D grooves, more elongation of macrophages was found in addition with higher expression of arginase-1 and IL-10 and lower levels of TNF- α , as compared to 2D wrinkles and flat surfaces. Also, the 1D wrinkles and flat materials were studied *in vivo* where it was found that the first one secreted greater values of arginase-1 close (0-50 μ m) to the implant but also at 50-150 μ m away of the implant, suggesting paracrine effects in the response (35).

2. Porous Scaffold Fabrication

The interest of developing scaffolds for tissue engineering with dual porosity structures has increased since they facilitate diffusion of nutrients and migration of cells (38,39). For the fabrication of such scaffolds, several techniques have been applied (41–43). For instance, particulate leaching, gas foaming, TIPS and additive manufacturing and their combinations are the most exploited for this purpose. In particulate leaching a water soluble porogen (e.g. salt), with a desired size, is added into a mold followed by the polymer solution, the solvent evaporates and porogens are dissolved in water, creating the pores (44). This technique has the disadvantages of porogen agglomeration or dispersion leading to uncontrollable size and shape of pores and their interconnectivity (43). Gas foaming consists of exposing the polymer to a high-pressure carbon dioxide gas to form the pores (44). However, this technique reveals low pore interconnectivity (41). TIPS techniques, besides the use of organic solvents, has the advantage of producing an interconnected pore structure in a simple and controllable manner, leading to homogeneous pore sizes and distribution that are function of the polymer concentration, solvent/non-solvent ratio and quenching temperature and time (45,46). This technique occurs by two possible mechanisms: solid-liquid or liquid-liquid phase separation where, in the former, the polymer and solvent interaction is strong as opposed to the latter. In both mechanisms, a polymer is solubilized in a solvent with low melting point. In the case of solid-liquid phase separation, it is the solvent crystallization that forms the porous structure. In the liquid-liquid either a non-solvent is added or the temperature is decreased to lower value than the solvent melting point to create instability and promote the phase separation (47,48). The cooling process affects the pore morphology

where poorly interconnected spheroidal pores or connected porous can be formed depending if the temperature is above (metastable region) or below (unstable region) the spinodal curve as seen in Fig. 2 (45,47).

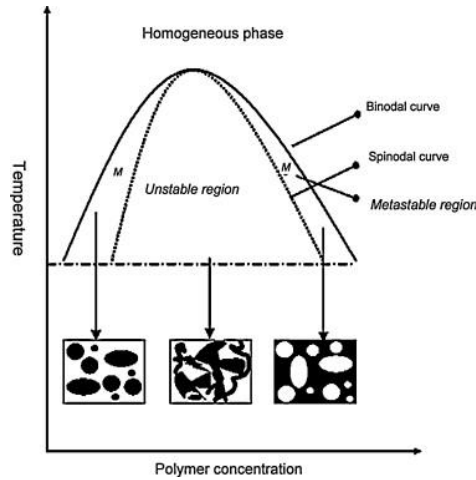


Figure 2 - Schematic temperature–composition phase diagram of a binary polymer solution. Adapted from (47)

A combination of TIPS and additive manufacturing enables a more controllable morphology and uniform pore structure and, has been revealed as a promising technique to fabricate scaffolds with wide range of morphological tunability. Di Luca and his colleagues have shown that surface topography can be controlled by this method by changing the gel concentration, temperature of solvent exchange (0°C, -56°C and -80°C) and non-solvent used (water, isopropanol, methanol, ethanol, n-hexane) (42). Also, this technique was applied for the fabrication of scaffolds with stiffness memory by solid-liquid phase separation and it was possible to regulate porosity and stiffness relaxation (49,50).

As 3D-TIPS has given proof of its tunability, this could be a great approach for immunomodulatory scaffolds by tuning their morphological properties. Therefore, the main goal of this project is to create 3D printed scaffolds with dual porosity and controllable topography that can tune the foreign body response. In particular, the main focal points of this work are: fabrication of a scaffold by 3D additive manufacturing combined with TIPS with different concentrations and molecular weights of PCLLA; evaluation of cytotoxicity and morphology changes of macrophages and analysis of polarization of macrophages that could potentially lead to pro-regenerative environment.

2. Materials and Methods

2.1. Materials. Three different poly (D,L-lactide-co-caprolactone) (PCLLA) based copolymers were used to fabricate scaffolds via additive manufacturing. The first copolymer contained a 68 / 32 ratio of lactide / caprolactone monomer with a 15 / 85 ratio of D / L lactide enantiomers and was obtained from Polyganics B.V. (Groningen, The Netherlands) and it is abbreviated to “PG” in this report. A second and third copolymers were obtained from Corbion, PURASORB® PLC 7015 and PURASORB® PLC 7038, both with a lactide / caprolactone ratio of 70 / 30 and a 0 / 100 ratio of D / L lactide enantiomers but, with different inherent viscosities (and thus molecular weight) of 1.5 and 3.8 dl / g, respectively. They are here referred as to “CB7015” and “CB”.

2.2. Scaffold Fabrication. The scaffolds were prepared by the combination of additive manufacturing and TIPS. Gels of PCLLA with different polymer concentrations, 5%, 7% and 9% (w/v) were first prepared in an 87% (v/v) 1,4-dioxane (Acros Organics, Thermo Fisher Scientific) solution in deionized water. For that, PCLLA was dissolved in 1,4-dioxane by stirring at RT and let it rest overnight, for PG and CB7015 while the CB was used directly after dissolution. Next, deionized water was added to the solution and kept stirring at 60°C until the solution became transparent, overcoming the cloud point which was usually 1 hour. Afterwards, the gel was immediately placed in the fridge for at least 2 hours. Thereafter, the gel was extruded with a pressure driven Biplotter system Enviosiotec at a 90° pattern with a 1000 µm fiber spacing and 0,2 mm layer thickness and a travel speed of 200 rpm to form 20 mm×20 mm×4 mm scaffolds. The gel was extruded through a needle of 0.8mm of inner diameter at 0.5-1 bar and 1.0-1.5 bar of pressure for 5% (w/v) and 7% (w/v) polymer concentrations, respectively. Then the scaffolds were stored at -80°C and freeze dried in FreeZone 2.5 Liter Benchtop Freeze Dry System (Labconco). As a control, non-porous scaffolds were fabricated via fused deposition modelling with a Bioscaffolder SYSENG using the same parameters as indicated above with a melting temperature of 195 and 200 °C for PG and CB7038, respectively and, with a G22 needle (400 µm internal diameter).

2.3. Scaffold Characterization.

2.3.1. Scanning Electron Microscopy (SEM). The morphology of the scaffolds was characterized by SEM analysis on a FEI/Philips XL30. Samples of approximately 4 mm x 4mm were cut from the full scaffolds using a scalpel and mounted on a SEM pin stub of 12 mm diameter and with the use of double-sided carbon adhesive (PELCO Tabs™, Ted Pella, Inc). Mounted samples were then gold sputtered with a Cressington Sputter coater 108 Auto. The samples were then imaged at a typical acceleration voltage of 10 kV.

2.3.2. Contact Angle. For surface characterization, water contact angle was measured using the sessile drop method at room temperature. The water contact angle, of a 4µL drop was measured in 5 replicas of each condition with Drop Shape Analyzer - DSA30 (KRÜSS GmbH).

2.3.3. Gel permeation chromatography (GPC). GPC was used to study the differences in molecular weight between the two polymers (CB7038 and PG) and, before and after scaffold fabrication. Samples were dissolved at concentration of 2 mg / mL in dimethylformamide (DMF, Sigma-Aldrich) containing 0.1 wt % LiBr and then passed through a 0.2 μ m filter. The molecular weights of samples were measured with a Shimadzu GPC equipped with a Shodex KG-G 4 Å guard column (4.6*10 mm) with 8 μ m beads, a Shodex KD-802 (5 μ m, 8*300 mm) column and a KD-804 (7 μ m, 8*300 mm) column in series. DMF was used as a mobile phase at a flow rate of 1ml/min. 15 μ L of sample was injected for each measurement.

2.3.4. Mechanical Properties. The compressive modulus of the scaffolds was determined using a TA Eletroforce 3200 mechanical tester equipped with a 450 N load cell at a displacement rate of 0.01 mm / s (n=3). The Young's modulus was calculated from the elastic regime of the curve.

2.3.5. X-ray micro computed tomography (micro-CT). X-ray microtomography imaging was conducted on 4 mm x 4mm x 4mm samples to characterize the scaffold microarchitecture on a Bruker micro-CT system using a slice thickness of 6 μ m.

2.3.6. Laser profilometry.

The surface of the scaffolds was measured by scanning them on a Keyence-VK-X260K laser profilometer over an area of 4 mm x 4 mm x 4 mm. From the scan of each material, the Sa (Arithmetical Mean Height) surface values were obtained from 3 random transverse profiles on each condition.

2.4. Support Bath. The support bath was intended to support the shape of the scaffold while printing. Two systems were tested: Lecithin / Glycerol / n-decane and Gelatin / Glycerol / water. For the lecithin system the protocol was adapted from and briefly consists of dissolving lecithin in n-decane and glycerol at 60°C stirring overnight and storing at 4°C until printing (51) with concentrations varying from 5 % to 80 % (w/v) of lecithin and from 1 % to 3 % (v/v) of glycerol. The gelatin system was tested with concentrations varying from 1,4 % (w/v) to 2.2 % (w/v) and 10 % (v/v) to 40 % (v/v) of glycerol. Briefly gelatin was mixed with glycerol and water for 1 hour stirring at 50°C and let it cool a stored at RT to reach homogeneity for 1 week or stored at 4°C for 2 hours.

2.5. Cell Culture. NR8383 cells (ATCC® CRL-2192™), a semi adherent rat alveolar cell line, were obtained by American Type Culture Collection (ATCC) and cultured in 85 % (v/v) of Ham's F12K medium with 2 mM L-glutamine adjusted to contain 1,5 g/L sodium bicarbonate and 15% of heat inactivated fetal bovine serum (FBS) at an initial density of 1 x 10⁵ cell / mL. Fresh media was added every second day and cells were subcultured when the cell density in suspension reached 4 x 10⁵ cell / mL.

Human bone marrow derived stromal cells (Dr. Prokop, donor 801.1), were cultured in MEM Alpha Medium supplemented with GlutaMAX, 10% of FBS and 1% of

penicillin/streptomycin (Gibco, Thermo Fisher) at an initial density of 10^3 cell / cm^2 and until 70 % confluence. Experiments were conducted at cell passage 5.

2.6. Cell culture on spin-coated polymer films. For the 2D cell experiments, a layer of polymer was formed on top of pre-cleaned (boiled for 2h in benzyl alcohol and sonicated in an ethanol solution) 18 mm glass coverslips by spin coating. The polymer was dissolved in chloroform at a 10 mg / mL concentration and 50 μL were dispensed over 10 seconds while the glass rotation speed was set at 900rpm. The rotation speed was then increased to 1800rpm and kept for 30s for solvent evaporation. For cell culture, the coverslips were sterilized by immersing them for 10 minutes in 70% of ethanol and then washed 3 times in PBS. Macrophages were seeded on the coverslip at 10^5 cells / mL in normal media and let adhered for 24h.

2.7. 3D Cell Culture. Additive manufactured scaffolds were cut for cell culture in 4mm x 4mm x 4mm with the use of a scalpel. For cell culture, the scaffolds were sterilized 15 minutes in 70% of ethanol, washed 3 times with PBS and transferred to new non-treated 24 well plates. 4×10^5 cells per scaffold in complete media (25 μL) were added on top of each scaffold and incubated at 37 °C under 5% CO_2 for 2 hours. The scaffolds were then flipped and incubated for another 2 hours. After a total of 4h after seeding, 1 mL of complete media was added to each well. Cells were incubated for 3 days prior to analysis for cell infiltration, morphology, cytokine secretion, cytotoxicity and DNA content analysis. The scaffolds tested were CB with 5 % (CB5) and 7% (w/v) (CB7) of PCLLA, PG with 5 % (PG5) and 7% (w/v) (PG7), and the FDM scaffolds: CB100 and PG100.

2.8. Macrophage polarization. Macrophages were polarized to M1 or M2 via stimulation with 10 ng / mL Lipopolysaccharide (LPS) and IFN- γ each or with 20 ng / mL of IL-13 and IL-4, respectively (all cytokines were acquired from Preprotech). M0 macrophages were non-stimulated.

2.9. Live/Dead. The cell viability was visualized after 48h of cell culture in 2D substrates by fluorescence microscopy with the calcein / ethidium bromide homodimer Live/Dead staining kit (Thermofisher) which was used following manufacturer instructions. In brief, each sample was washed with 1x PBS and incubated in 1mL of a solution of 1 μM of calcein and 0,25 μM of ethidium homodimer-1 for 30 min at 37°C under 5% CO_2 and imaged by an inverted microscope Nikon Eclipse Ti, equipped with Andor Zyla sCMOS camera. The number of live and dead cells in each of three images per sample was counted and the percent viability was calculated by dividing the number of live cells by the number of total cells per image ($n = 3$).

2.10. Lactate dehydrogenase (LDH) Assay. The cytotoxicity of the materials was quantitatively measured by the release of lactate dehydrogenase by the macrophages culture on spin-coated polymer films. The LDH assay (Pierce LDH Assay, Thermo-Fisher) was performed following the manufacturer's instructions. As negative control (0% LDH release), macrophages were culture on 24-well plates at the same density. For positive controls (100%

LDH release) macrophages cultured under identical conditions on 24-well plates were lysed using the 10x Lysis Buffer in a 1:100 dilution and incubated at 37°C, 5% CO₂ for 45 minutes. The media was recovered and stored at 4°C until further use for a maximum of 3 days. The calculation of %Cytotoxicity was made by the following formula:

$$\% \text{ Cytotoxicity} = \frac{[\text{Sample} - \text{Average of Negative Control}]}{[\text{Average of Positive Control} - \text{Average of Negative Control}]} \times 100$$

2.11. Quantification of DNA. Total DNA was quantified using CyQuant Assay kit (ThermoFisher) to assess cell adhesion and proliferation. Samples (n=3), after 48 hours of culture, were washed with PBS to remove non-adhered cells. Adherent cells were scraped from the well, transferred to an Eppendorf tube and centrifuged at 200 rcf for 5 min. Supernatant was removed and cells were frozen at -80°C. Cells were then frozen in liquid nitrogen and thawed at 56°C for 3 times. Samples were then digested with 1 mg / ml proteinase K in Tris / EDTA buffer (pH 7.6) overnight at 56°C. Afterwards samples were freeze-thawed again 3 more times. Fluorescence was measured at emission wavelength 520nm using a multiplate spectrophotometer Clariostar (BMG LABTECH) and DNA concentrations were calculated from a λ DNA standard curve.

2.12. Immunofluorescence. The samples after 48 hours of culture in 2D substrates or 3 days in 3D scaffolds, were fixed with 4% paraformaldehyde in PBS for 15 minutes at room temperature and then washed twice with PBS. The samples were then permeabilized with 0,1% Triton X-100 for 10 minutes and washed twice with PBS. The samples were blocked with 3% of bovine serum albumin (BSA) and 0.01% of Triton X-100 for 1 hour at room temperature and washed 3 times with the washing buffer, consisting of 1:10 dilution of the blocking solution describe above. Cells were then incubated overnight at 4°C with rabbit Anti-Paxilin (Sigma Aldrich) 1:200, rabbit Anti-Arginase (Invitrogen) 1:100 or mouse anti-iNOS 1:500. Then, samples were washed 3 times with washing buffer. Samples were later incubated at room temperature for 1 hour with the secondary antibodies anti-rabbit Alexa Fluor-488 donkey or anti-mouse Alexa Fluor-647. For analysis of the cytoskeleton (F-actin) cells were stained with Alexa Fluor-568 conjugated phalloidin. All the samples were counterstained with 1 mg / ml Hoescht dye at a 1:2000 dilution for 10 minutes, washed with washing buffer and maintained on PBS, and then imaged with Nikon Eclipse Ti, equipped with Ander Zyla sCMOS camera or a Leica TCS SP8 confocal microscope with 63x oil objective for 2D experiment and 25x water objective for 3D experiments. For 3D experiments Z-stacked images were acquired by scanning throughout 1.5 mm thickness of the scaffolds at 2 μ m/Z-step.

2.13. SEM of cell cultures on scaffolds. For SEM analysis, samples were dried via immersion on an ethanol dilution series in PBS (50%, 70%, 80%, 90%, 96% and 100%) with 15 minutes incubation at room temperature for each dilution. Then, 98% hexamethyldisilazane (Alfa AesarTM, ThermoFisher) was added to the samples and incubated for 15 minutes at room temperature. Samples were then air-dried overnight. Dry

samples were then gold sputtered (Cressington Sputter coater 108 Auto) before SEM analysis.

2.14. Cytokine secretion. The secretion of TNF- α (Biogems, Prepotech)), IL-10 (R&D Systems) and TGF- β (Abcam) was measured following the manufacturer's protocol. The absorbance was measured on a Clariostar (BMG LABTECH) plate reader. For the standard curve, a dilution series of the cytokines was produced and measured. A four-parameter logistic (4-PL) regression was generated.

2.15. *In vivo* Experiments. For *in vivo* investigation, scaffolds with 4 mm x 4 mm x 4mm were prepared for CB7 and PG7, CB100 and PG 100. The animal experiment was approved by the Dutch Central Committee on Animal Testing (CCD). Athymic nude rats (CrI: NIH-Foxn1^{rmu} 316 rat) were obtained from Envigo in the experiment. Animals were housed at 22 °C with a 12 h light/dark cycle and had ad libitum access to water and food. Only male rats were used in the formal study. The animals (N=7) were anesthetized by inhalation of isoflurane. The dorsal surgical sites were shaved, disinfected and incised. Four subcutaneous pockets were created for the insertion of scaffolds. After implantation, incisions were closed with sutures. Analgesics were administrated with Buprenorphine (Buprecare, 0.05 mg/kg, SC) and Carprofen (4mg/kg, SC). Animals were routinely monitored after the operation.

2.16. Statistical Analysis. All data is presented as mean \pm standard deviation (SD) and statistical significance was measured by performing a one-way ANOVA analysis followed by Tukey's multiple comparison using GraphPad, Prism Software (V.6). Differences were taken to be significant for $p < 0.05$.

3. Results and Discussion

3.1. Fabrication of PCLLA 3D-TIPS scaffolds

PCLLA is a copolymer of ϵ -caprolactone and lactide and its individual monomers give rise to biocompatible and biodegradable polymers. Their copolymerization overcomes some limitations of the individual homopolymers (52). Polycaprolactone (PCL) is a hydrophobic and semi-crystalline polymer with a melting point of 59-64°C and a glass transition at -60°C. Its degradation time is from 2 to 4 years and it is soluble in chloroform, 1,4-dioxane, dichloromethane and tetrahydrofuran (THF). Polylactide (PLA) has three different forms, the crystalline ones being produced out the individual enantiomeric forms - D (PDLA) and -L lactide (PLLA), and the mostly amorphous, from the racemic form, D, L. The melting point of PDLA and PLLA (130°C to 180°C) and glass transition (40 to 70°C) vary with the molecular weight. As PCL, PLA is also soluble in chloroform, 1,4-dioxane, dichloromethane and tetrahydrofuran (THF) (53). It has been reported that the copolymerization of ϵ -caprolactone and lactide or lactic acid increases the crystallinity, decreases the elastic modulus and enhances the flexibility of the PLA homopolymer (54). In this report, two copolymers with different composition are used, where the first, coded as PG, has a 70 / 30 (wt.% / wt.%) ratio of lactide / ϵ -caprolactone monomers and the second, coded as CB, has 68 / 32 ratio of lactide / ϵ -caprolactone monomers. Only the PG 70 / 30 has both enantiomers (15 wt. % -D and 85 wt. % -L) while CB is made of only -L form lactide. These polymers were chosen for their chemical similarities but expected differences in crystallinity and thus, mechanical properties.

In order to evaluate other parameters that can affect macrophage adhesion and overall immune response, the wettability of the materials was studied by water contact angle (WCA). The results showed a WCA of $78,20 \pm 2,277$ for PG and $78,06 \pm 3,225$, indicating that they are both hydrophobic with similar contact angles (Figure 6A).

For the fabrication of the scaffolds, a solution of PCLLA with the solvent 1,4-dioxane and the non-solvent water was jellified leading to polymer chain entanglements before printing. For a stable gel suitable for printing a certain molecular weight and viscosity are necessary. In this technique, the porosity is given by the phase separation between water and 1,4-dioxane upon freezing and freeze dried the water droplets.

Two different ratios of solvent / non-solvent, 90 / 10 vol. / vol. and 87 / 13 vol. / vol, were tested with the PG polymer (Figure 3A, B). Two concentrations of the polymer were evaluated, 5 and 7 wt. %. For both concentrations of the polymer, the ratio 90 / 10 vol. / vol presented flatter and less defined fibers in comparison with 87 / 13 vol. / vol. ratio. So, the latter ratio was chosen for this study.

Two different CB copolymers, with equal composition but different inherent viscosities were tested. Gels of CB 7015 (low viscosity) at 7 % (w/v) concentration of the polymer were printed. As shown in Figure 3C, the scaffolds did not show a distinguishable pattern as the gel coalesced while printing. However, they presented porosity in the cross-

section. This result could be due to the low inherent viscosity (1.2 - 1.8 dl/g) of the copolymer, and thus low molecular weight. We then tested CB 7038, which has higher inherent viscosity (3.3 – 4.3 dl/g). These gels were capable of retaining the shape of the fibers upon printing (Figure 5A, B).

Since it has been reported that the concentration of the polymer in TIPS affects material porosity (45,55), in this report, three different polymer concentrations of 5, 7 and 9 wt. % were evaluated and compared in terms of morphology of scaffolds and microporosity by SEM (Figure 3D,E,F). Scaffolds fabricated from 9 wt. % polymer gels showed the best defined fibers. However, the printing process was more difficult than with other gel concentrations since it needed high pressures (higher than 4-5Pa) to extrude the gel with the same needle diameter, reaching the limitations of the equipment. Therefore, the next experiments were done with 5 and 7 wt. / vol. % PG or CB7038 polymer. Figure 5 shows representative SEM micrographs of the fabricated scaffolds. From the images, it is evident that 3D-TIPS scaffolds (Figure 5A, B, D, E) have microporosity within the fibers as opposed to scaffolds fabricated by fused deposition modelling (FDM), in Figure 5C,F. The lowest polymer gel concentrations lead to scaffolds with flattered fibers and this interferes with the height of the scaffold. Between the two polymers, the one with higher crystallinity, CB, showed better retention of the lattice shape as compared to PG which presents more staggered fibers. The CB5 and CB7 scaffolds presented pores with diameter of $22,82 \pm 13,96 \mu\text{m}$ and $18,12 \pm 11,84 \mu\text{m}$, respectively, while PG 5 and PG7 have $23,49 \pm 52,49 \mu\text{m}$ and $13,23 \pm 8,13 \mu\text{m}$, respectively. All of the scaffolds showed higher variance between the diameters of pores, suggesting a heterogeneity on microporosity (Figure S4).

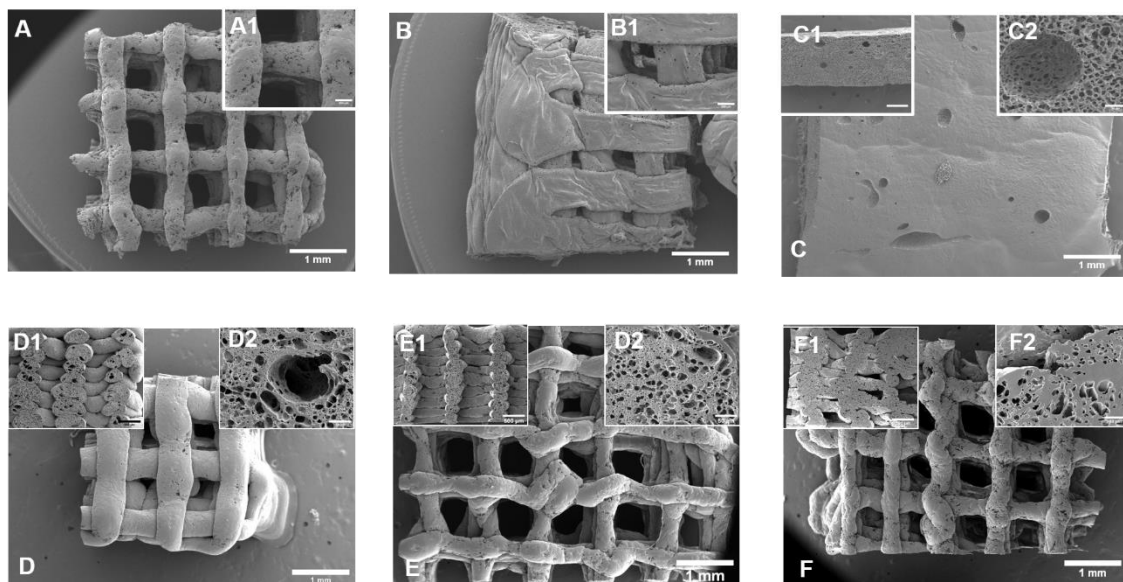


Figure 3 – SEM images of the 3D TIPS scaffolds. Axial view of the A) 7% PCLLA PG with 87%/13% ratio of 1,4 dioxane/water; B) 7% PCLLA PG with 90%/10% ratio of 1,4 dioxane/water; C) 7% PCLLA CB7015 with 87%/13% ratio of 1,4 dioxane/water; D) 5% PCLLA PG; E) 7% PCLLA PG; F) 9% PCLLA PG. Fibers

inset in A1 and B1, and cross-sectional views in the upper corners of C, D, E, F. A1-C1 scale= 200 μ m, C1-F1=500 μ m, C2-F2 scale =50 μ m

The structure of the scaffolds, internal fiber microporosity, porosity total open pore volume and surface area were analysed by μ -CT (Figure 4 and Table 1). As opposed to some literature about TIPS technique, which states that the increase of polymer concentration decreases the percentage of total porosity (45,55), here the 7 % (w/v) scaffolds show highest values of porosity (Table 1). Since the technique is a combination with additive manufacturing, other factors affect total porosity such as fiber spacing. As stated, the fibers of 7 % scaffolds are better defined that the ones in their 5 % counterparts, both for CB and PG, leaving a bigger space between the fibers, on the xy plane, which increases the total porosity. In addition, all 3D-TIPS scaffolds showed higher values of open porosity, revealing a great pore interconnectivity essential for tissue and vascular infiltration. The lower concentrations revealed higher total surface area comparing to 7% concentrations which could mean in a higher cell retention.

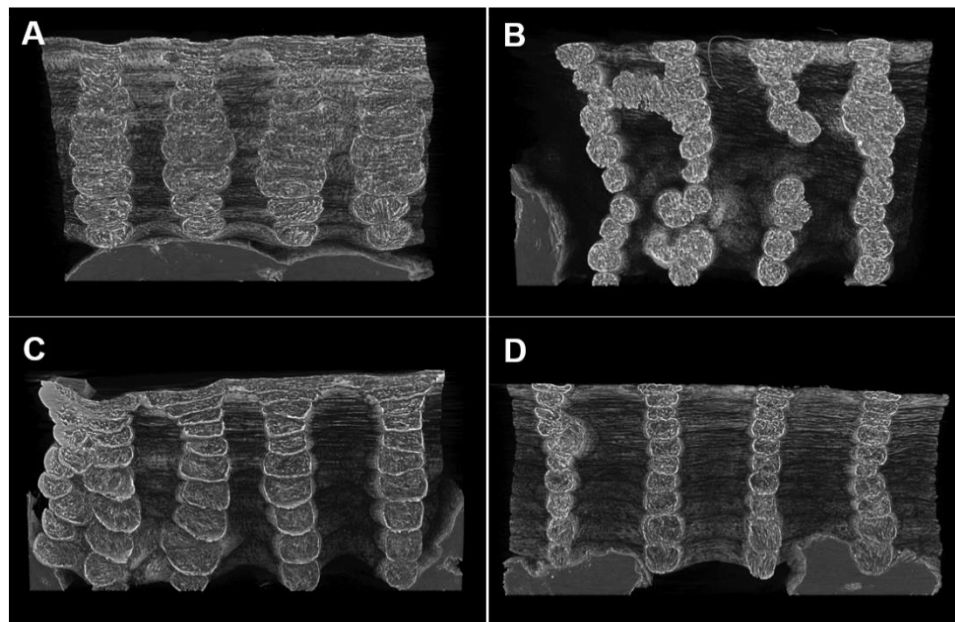


Figure 4 - Representative images of μ -CT analysis of A) 5% PG, B) 7%PG, C) 5% CB and D) 7% CB.

Table 1 – Total porosity, Open Porosity, Total surface and connectivity are measured by μ -CT analysis for CB5, CB7, PG5 and PG7. For CB100 and PG100 the theoretical total porosity was calculated. For total surface area all the conditions were normalized considering a volume of 10mm³.

	CB			PG		
	5	7	100	5	7	100
Porosity (%)	61,536	69,191	39,9	53,330	60,986	5,75
Total open pore percent (%)	61,532	69,168	-	53,327	60,975	-

Total surface area (mm²)	6,21E-02	4,04E-02	-	7,09E-02	5,10E-02	-
Connectivity	560301	437494	-	481655	218375	-

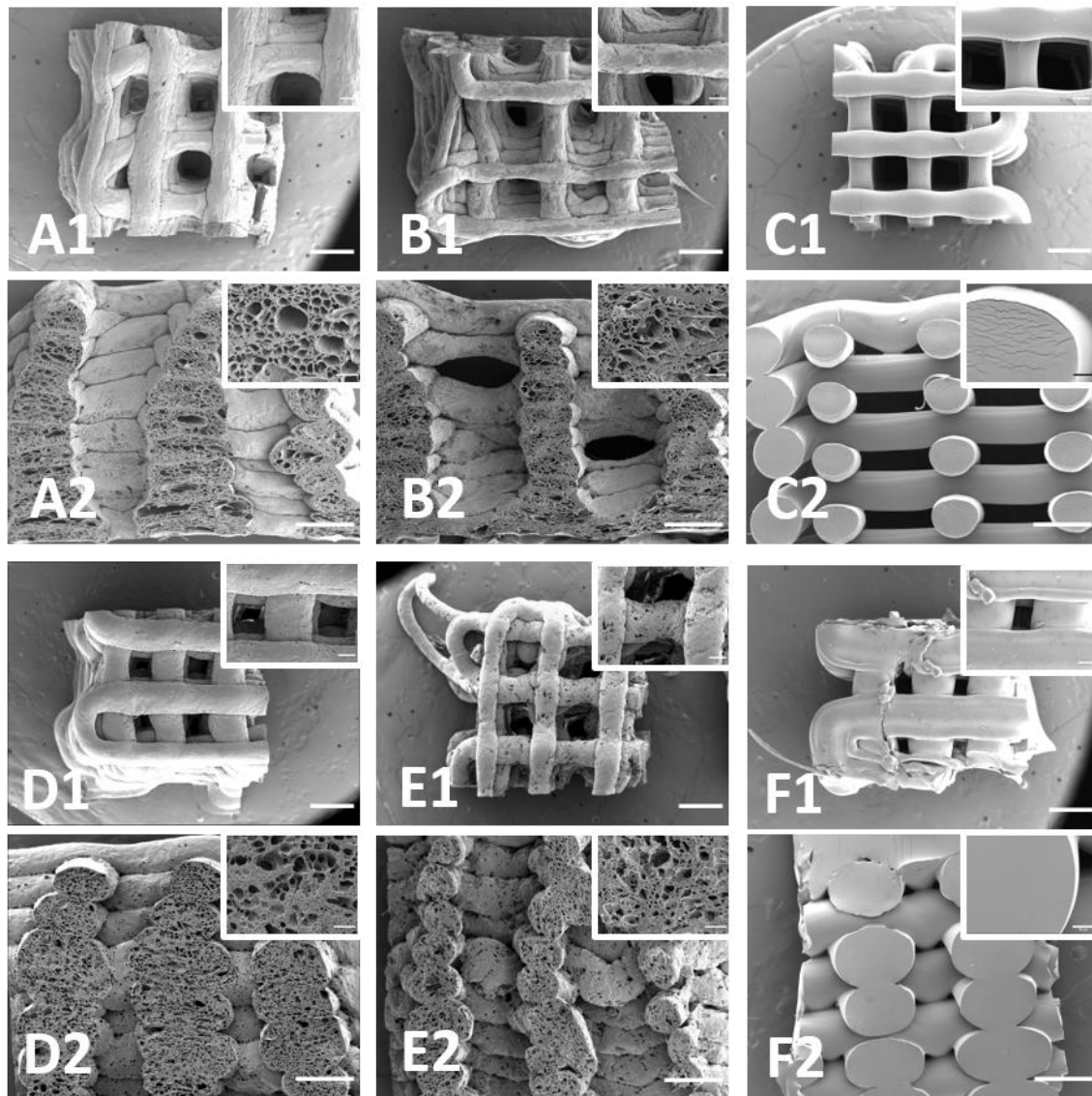


Figure 5 - Representative images of the scaffolds from the axial and cross section with A) 5%CB, B) 7% CB, D) 5% PG and E) 7%PG and the FDM scaffolds from CB (C) , and PG (F). The images of fiber geometry are in upper corner of A1-F1, scale=200μm and the porosity inside the fibers of A2-F2, scale=50μm.

As the 7 % scaffold displayed higher levels of porosity and more defined fibers, the following characterization and cell work were only relative to these scaffolds, as compared to non-porous FDM scaffolds.

The surface roughness of the scaffolds, what cells will first be in contact with, was evaluated by profilometer analysis. As expected from the SEM images, the 3D-TIPS

scaffolds had a greater surface roughness (Sa) than the conventional scaffolds (Figure 6C,D). For CB100 $6,418 \pm 1,283 \mu\text{m}$, CB7 $31,35 \pm 18,05 \mu\text{m}$, PG100 $2,933 \pm 0,3027 \mu\text{m}$ and PG7 $17,12 \pm 4,430 \mu\text{m}$. This values are related to the surface that cell can interact, which means that CB7 and PG7 showed higher surface area. The higher roughness on 3D-TIPS has already been shown by Di Luca et.al where they also studied how roughness is affected by changes in temperature, solvent and non-solvent used (42).

The influence of 3D-TIPS technique and the composition of the polymers (more amorphous PG or more crystalline CB) on the mechanical integrity was tested by compression tests. Stress-strain curves of 3D-TIPS scaffolds fabricated from 7 % (w/v) gels of CB and PG and, FDM scaffold controls (CB100 and PG100) are shown in Figure 6F. CB polymers had a higher compressive strenght than PG and, the scaffolds from 3D-TIPS had lower compressive strenght than those produced by FDM. The Young's modulus in compression (E) was calculated from stress-strain curves and was greater in the more crystalline polymers (CB) than the amorphous ones (PG) and in 3D-TIPS than in FDM scaffolds. Values of E of CB100 ($404,1 \pm 112,5 \text{ kPa}$), CB7 ($42,75 \pm 21,07 \text{ kPa}$), PG100 ($4,933 \pm 1,511 \text{ kPa}$) and PG7 ($3,5 \pm 1,593 \text{ kPa}$) were measured for stiffness comparison. Furthermore, the yield stress of CB100 was $734,6 \pm 53,99 \text{ kPa}$, CB7 was $57,7 \pm 18,3 \text{ kPa}$, PG100 was $9,5 \pm 2,86 \text{ kPa}$ and PG 7 was $6,4 \pm 2,25 \text{ kPa}$. These results show that, not only the semi-crystalline characteristics of the polymer affect the stiffness of a material, but also its porosity, since CB7 and PG7 showed lower values than its counterparts.

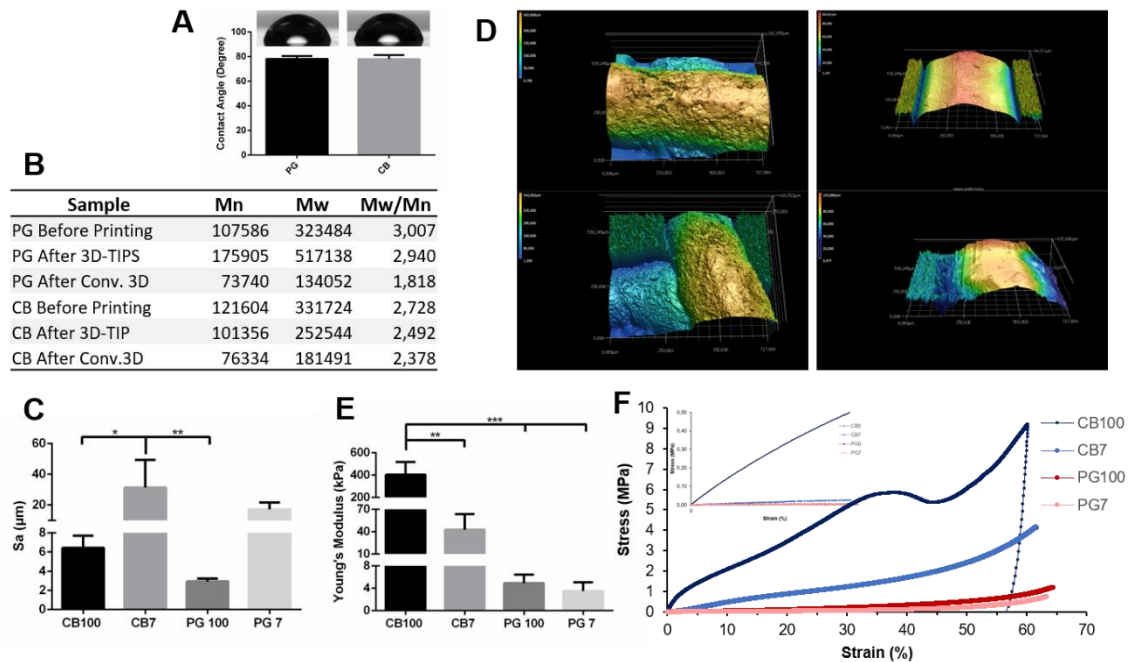


Figure 6 - Wettability (A) and physical properties of all the scaffolds. B) indicates the data from GPC analysis, C) Surface Roughness, D) Representative images of surface roughness where Left up: CB7, Right up: CB100. Left down: PG 7 and right down: CB100.

From previous studies on 3D-TIPS scaffolds, our values of total porosity are lower than what they present (around 95%). That study, even if it presents great results in terms of porosity, shape controllability and mechanical properties, is an indirect method of 3D printing where a mould is used to form the shape of the scaffold (49). From our data it is shown a fabrication of scaffolds with simple few steps that presents great pore interconnectivity, higher roughness, higher porosity and less stiff than FDM scaffolds. Even if it needs some improvements in terms of shape controllability, this technique shows a promising way to fabricate scaffolds with tuneable properties, which can be further selected depending on the final tissue application.

3.2. *In vitro* cellular response to PCLLA polymer films

To evaluate the biocompatibility of the materials used here, macrophages were seeded on spin-coated films of PG and CB as well as tissue culture plate controls (TCP) for 48 hours. For that, a solution of PCLLA in chloroform was spin coated and a monolayer of polymer was formed in a cover slip. The cell viability was measured by a Live / Dead assay based on calcein and Ethidium homodimer represented in Figure 7A, C. In this assay, live cells are detected since they have intracellular esterases that convert Calcein-AM into a green fluorescent calcein (ex/em ~495 nm/~515 nm). Dead cells, without esterase activity, are stained by Ethidium homodimer (EthD-1) that enters damaged cell membranes and binds with the nucleic acids, producing a red fluorescence in dead cells (ex/em ~495 nm/~635 nm). The amount of live and dead cells was counted from the fluorescent images. Macrophages on PCLLA presented a 94.97 %, 98.07 % and 98.89% of viability, for PG, CB and TCP, respectively.

The cytotoxicity of the materials was evaluated as a measure of the lactate dehydrogenase (LDH) release of the cell when cultured on these (Figure 7, B). Both polymers induced low cytotoxicity, CB with $2,141 \pm 0,9217\%$ and PG with $1,181 \pm 1,125\%$, comparing to the positive control $100,0 \pm 9,120\%$. Both, live dead and LDH release assays, indicate that these polymers are biocompatible, and they do not affect the cell viability of macrophages.

The capability of macrophages to attach to the different copolymers was assessed by measuring the DNA content after 48h of culture on spin-coated films. Although a higher DNA content was measured on PG films (Figure 7.D), the detected differences between polymers (PG: $0,2052 \pm 0,08080 \mu\text{gDNA}$ CB: $0,1009 \pm 0,06072 \mu\text{gDNA}$) and control ($0,1043 \pm 0,02801 \mu\text{gDNA}$) in terms of cell adhesion, were non-significant. This result was already expected since that, in the characterization of the material, the wettability of both polymers (Figure 6A) was similar and so the adhesion of macrophages to the material would be equivalent.

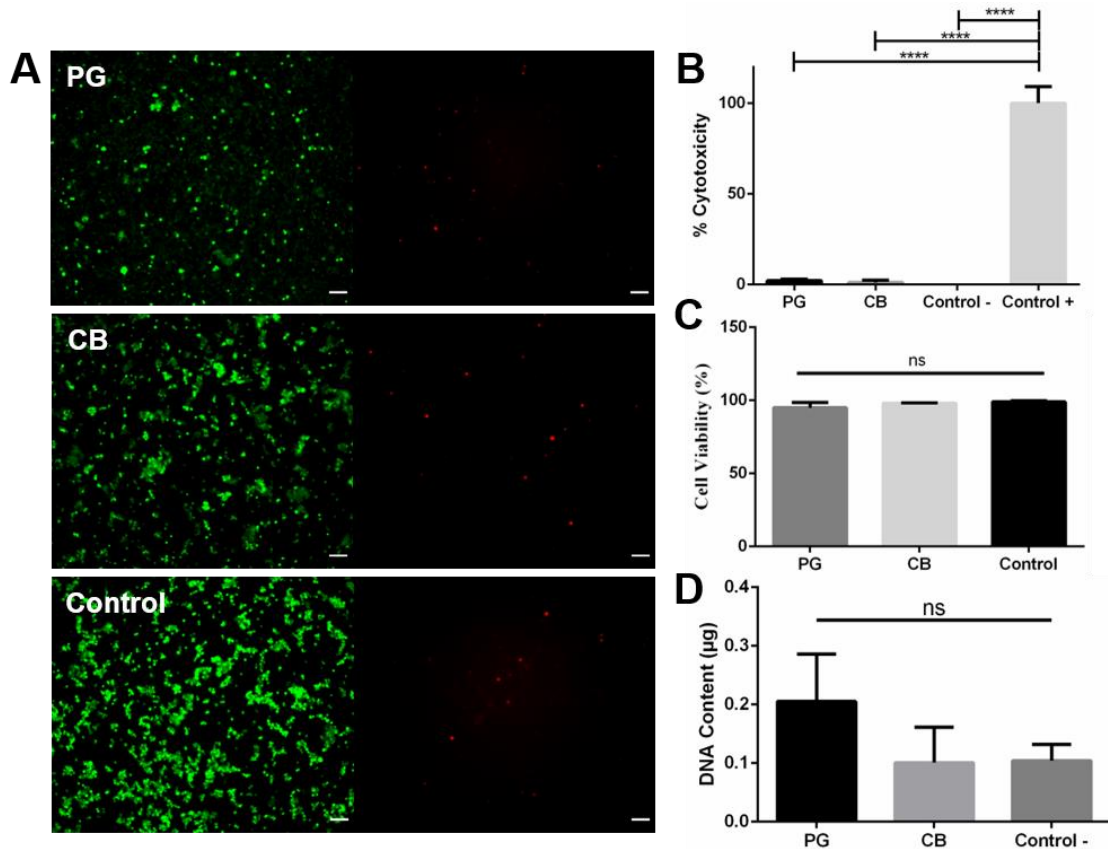


Figure 7 - Biochemical assays for assessment of cell viability by the materials (A, C), cytotoxicity (B) and cell attachment by the DNA assay (D), Scale bar= 100µm.

To analyse how macrophages attach to the materials and how its composition affects adhesion, F-actin and an adaptor protein, paxillin, were fluorescently stained and visualized via light scanning microscopy. Most of the cells interact with ECM by the maturation of focal adhesions, serving as mechanical links to the cells. On macrophages, these mechanical linkages are known as podosomes and differ by their cylindrical morphology, as opposed to the punctuated morphology of focal adhesions (20). No formation of podosomes was detected in the macrophages cultured on any of the different substrates (PG, CB or TCP) (Figure 8). One explanation for this result could be the lack of tension on the substrate. However, glass slides, used in 2D cell culture, have great values of stiffness and podosomes range from 0.5µm to 2µm of diameter, so the magnification used in this report might not have been sufficient for their detection (56).

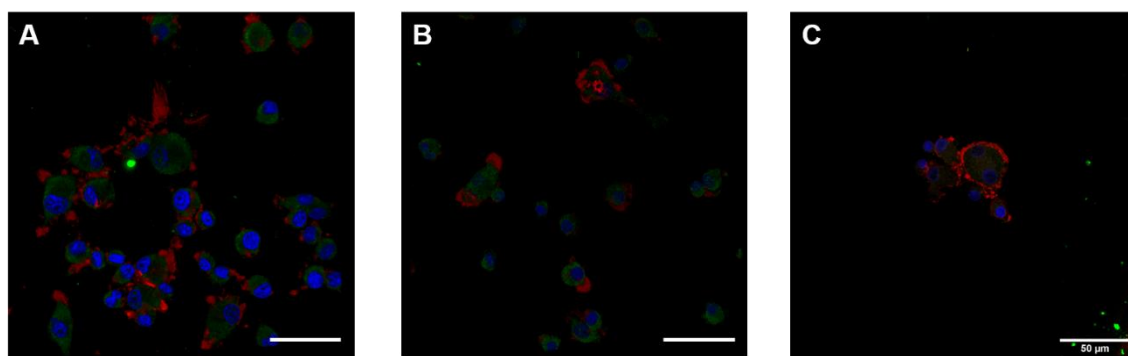


Figure 8 – Immunofluorescence images with staining of F-actin (red), Paxilin (green) and cell nuclei (blue) for PG (A), CB (B) and TCP, Scale bar=50μm.

In order to evaluate the influence of the chemistry of both polymers in macrophage polarization, an immunostaining of M1 and M2 markers was performed. The cells were stimulated, after 24 hours of adhesion, with LPS/IFN- γ (M1), IL-4/IL-13 (M2) or non-stimulated (M0) and stained with iNOS antibody and Arginase-1 antibody. These are two markers that are referred to distinguish between M1 and M2-like macrophages. Depending on the stimuli, macrophages use arginine to produce nitric oxide (NO) and citrulline by the iNOS enzyme (M1) or, ornithine and urea by the arginase-1 enzyme (M2). The former is typical of M1 macrophages and the production of NO enables the increase of cytotoxicity to eliminate pathogens such as bacteria. As biomaterials are a potential locus of bacteria and biofilms, an activation, like the microbial product LPS, mimicking the action of macrophages for the bacteria clearance is essential. With increase of arginase activity, characteristic of M2 macrophages, the final products are ornithine and urea. Ornithine, by the action of ornithine decarboxylase and ornithine aminotransferase, leads to the production of polyamines and proline, respectively (57). This consumption of arginine, blocks the continuation of inflammation and induces wound healing by the aforementioned production of proline, a precursor of collagen (57).

Different concentrations of cytokines were tested in order to find difference in the morphology of cells and the expression of arginase and iNOS. From the results shown in Figure S2 (supplemental information) equivalent intensity on the markers stained were detected on all concentrations. Therefore, the final concentrations for the rest of the tests were 10ng/mL for LPS/ IFN- γ and 20ng/mL for IL-4/IL-13. Furthermore, the effect of heat inactivation of FBS was tested in iNOS staining and it is shown in Figure S1. Heat inactivation of FBS is done to inactivate the complement proteins that are present in serum. These proteins, such as anaphylotoxins like C3a and C5a, influence the stimulation of phagocytosis and induce release of ROS by immune cells (1). The results show that, for M2 and M0 stimulated macrophages, the iNOS staining is less intense with heat inactivated FBS than non-heat inactivated FBS. This suggests that FBS non-heat inactivated was inducing a pro-inflammatory profile in macrophages even without pro-inflammatory cytokines. As such, for the next experiments, only heat inactivated FBS was used.

M1 stimulated macrophages cultured on PG, CB and TCP substrates expressed high levels of iNOS (Figures 10-12). Bright-field images revealed the formation of aggregates of macrophages, as opposed to M0 and M2 stimulated macrophages. Between M0 and M2 stimulated macrophages no evident differences, neither in morphology nor in markers expression, were observed. Both presented mostly rounded cells and few elongated ones and expressed both iNOS and arginase 1. Some reasons behind the lack of difference between M2 and M0 macrophages could be the concentration of cytokines, the method of cell fixation, or the antibody viability. The concentration of cytokines, as stated before, was tested but no differences between the highest and lowest concentration were observed on arginase staining. The method of fixation was also tested by comparing the influence of 4% PFA and cold methanol on the arginase staining and both expressed similar intensity of arginase. Two different antibodies of arginase were used throughout this project, but the staining remained the same. The similarities of morphology in M0 and M2 may indicate that it is the stimulation that is failing; since increasing the concentration does not change the expression of arginase, the cells could be not sensible enough for these cytokines and not express high levels of arginase. In addition, it has been shown that macrophages do not exhibit an evident profile between M1 and M2 making it necessary to further look for other markers and cytokines (33). From these results, PG expressed higher levels of arginase comparing to CB and lower levels of iNOS in all conditions than CB and control. This can suggest that PG polymer induces an anti-inflammatory response to macrophages. However, further quantification measurements are needed to distinguish the functions of macrophages on different polymers.

To further examine the phenotype of macrophages, their cytokine expression was measured in all tested culture conditions. TNF- α is a pro-inflammatory cytokine expressed mainly by M1 macrophages. M1 stimulated macrophages expressed higher concentrations of TNF- α than non-stimulated or M2 stimulated macrophages, as expected (Figure 9). M1 stimulated macrophages cultured on PG scaffolds had significant increase in TNF- α compared to non-stimulated macrophages and M2 macrophages cultured on PG, CB and TCP. This could suggest that the material induces a pro-inflammatory phenotype, however no significant difference compared to control was found.

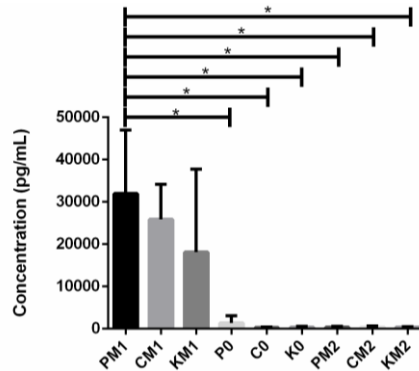


Figure 9 – TNF- α expression of macrophages in response to polymer films (P for PG and C for CB) or TCP (K) with 10 ng / mL LPS/IFN- γ (M1), 20 ng / mL IL-4/IL-13 (M2) or unstimulated (0).

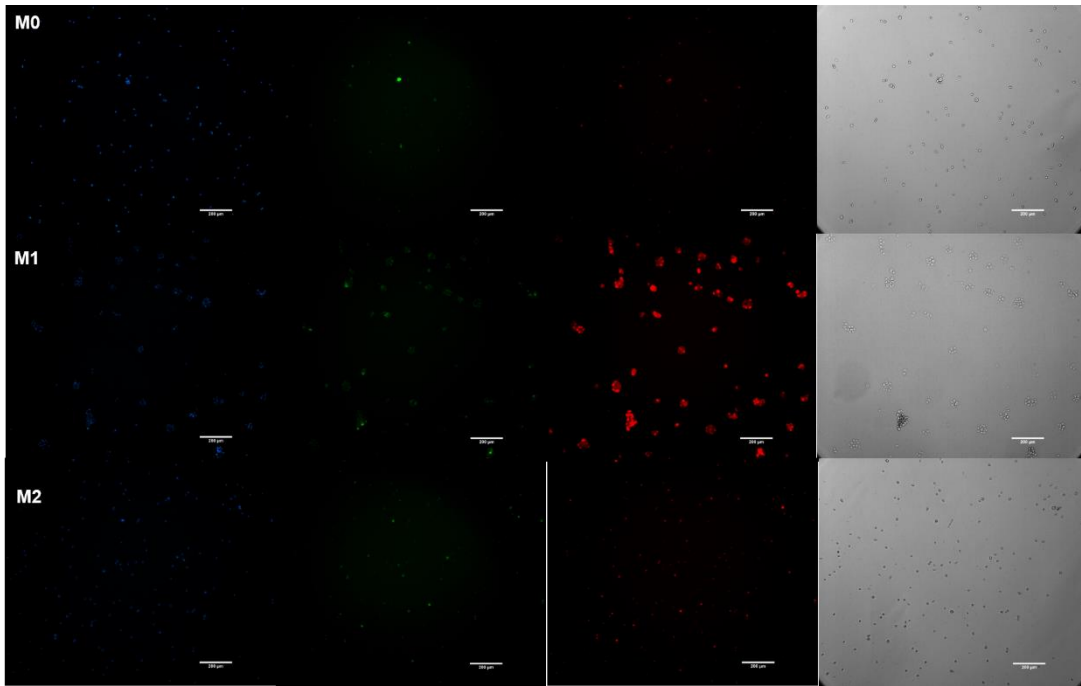


Figure 10 – IF and brightfield images of macrophages in response to TCP culture and 10 ng / mL LPS/IFN- γ (M1), 20 ng / mL IL-4/IL-13 (M2) or unstimulated (M0). Nuclei (blue), Arginase-1 (Green) iNOS (red) are represented. Scale bar=200 μ m

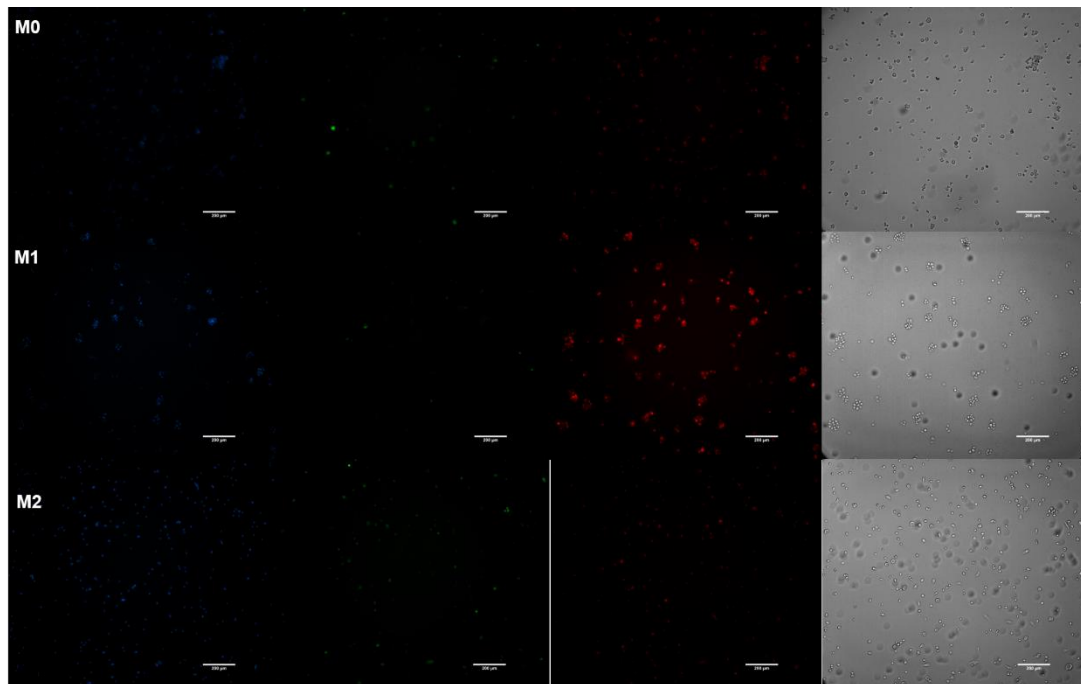


Figure 11 - IF and brightfield images of macrophages in response to CB culture and 10 ng / mL LPS/IFN- γ (M1), 20 ng / mL IL-4/IL-13 (M2) or unstimulated (M0). Nuclei (blue), Arginase-1 (Green) iNOS (red) are represented. Scale bar=200 μ m

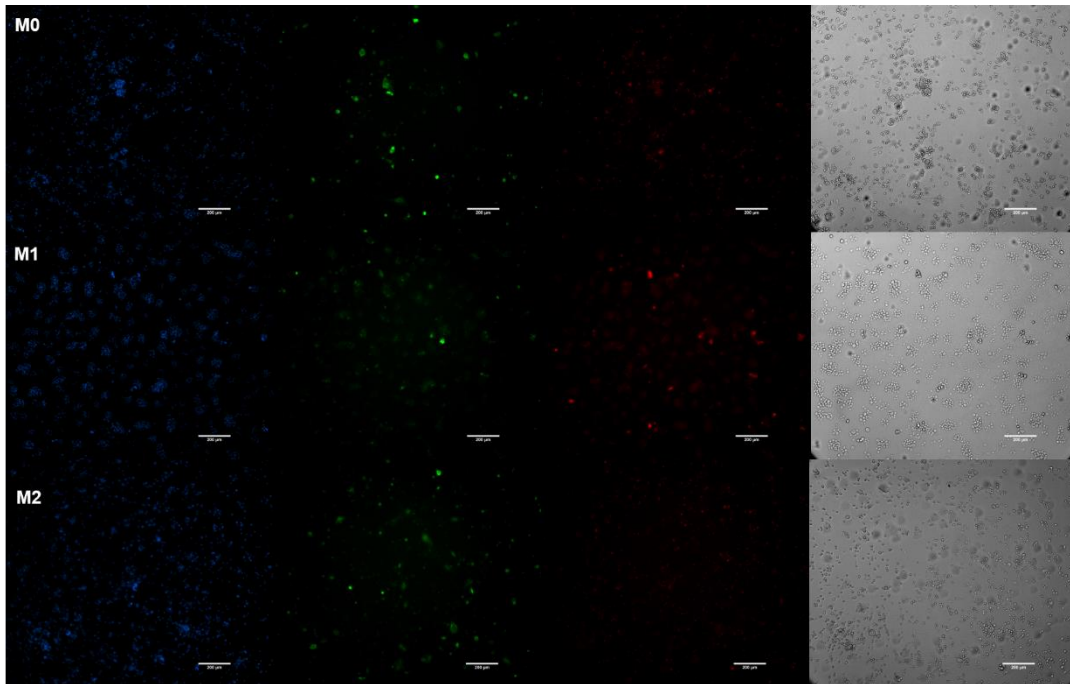


Figure 12 - IF and brightfield images of macrophages in response to PG culture and 10 ng / mL LPS/IFN- γ (M1), 20 ng / mL IL-4/IL-13 (M2) or unstimulated (M0). Nuclei (blue), Arginase-1 (Green) iNOS (red) are represented. Scale bar=200 μ m

3.3. *In vitro* cellular response to PCLLA scaffolds

To demonstrate whether surface topography and porosity influence the macrophage response, cells were seeded on scaffolds and cultured for 3 days. First, cell attachment and morphological changes were analysed on 3D TIPS scaffolds (5% and 7%wt) and FDM scaffolds by DNA quantification, immunostaining of F-actin and by SEM. After 3 days of culture, F-actin staining showed that FDM scaffolds had lower cell adhesion compared to 3D-TIPS scaffolds (Figure 13), which was further confirmed by DNA quantification (PG7: $1902 \pm 0,02976$; CB7: $0,3384 \pm 0,01090$; PG100: $0,01326 \pm 0,002525$ and CB100: $0,01593 \pm 0,005914$ μ g DNA) (Figure 16A). One possible explanation is the fact that 3D-TIPS scaffolds present higher surface roughness, and thus surface area, than conventional scaffolds; macrophages are known to adhere better on rough than smooth surfaces (20).

There were no evident differences in cell adhesion between the 3D-TIPS scaffolds of both concentrations (5% and 7%wt), suggesting that the differences in surface area (Table 1) are not sufficient to greatly affect macrophage attachment between scaffolds.

PG scaffolds appear to present higher number of cells attached than CB by fluorescent images of 3D-TIPS scaffolds with 7% (w / v) polymer concentration. However, DNA quantification demonstrated that CB supported more cell attachment. This could be related to more cell infiltration into the microporosity in CB scaffolds and less cell attachment on the surface of the fibers. Both polymers showed similar values of hydrophobicity, which indicates that in films cell attachment would be equivalent too, as shown in Figure 7D. However, from previous results, scaffolds from both polymers had distinct physical

properties. CB presents higher stiffness, from the elevated levels of compressive strength and Young's modulus, higher porosity and similar surface roughness compared to PG. From previous studies, higher stiffness materials (280kPa) showed increase cell proliferation of human monocyte-derived macrophages compared to the less stiff counterparts (1-5kPa) (24). Here, CB7 scaffolds with E of $42,75 \pm 21,07$ kPa had more cell adhesion than PG7 with E of $3,503 \pm 1,593$ kPa, which could be also related to cell proliferation during cell culture period.

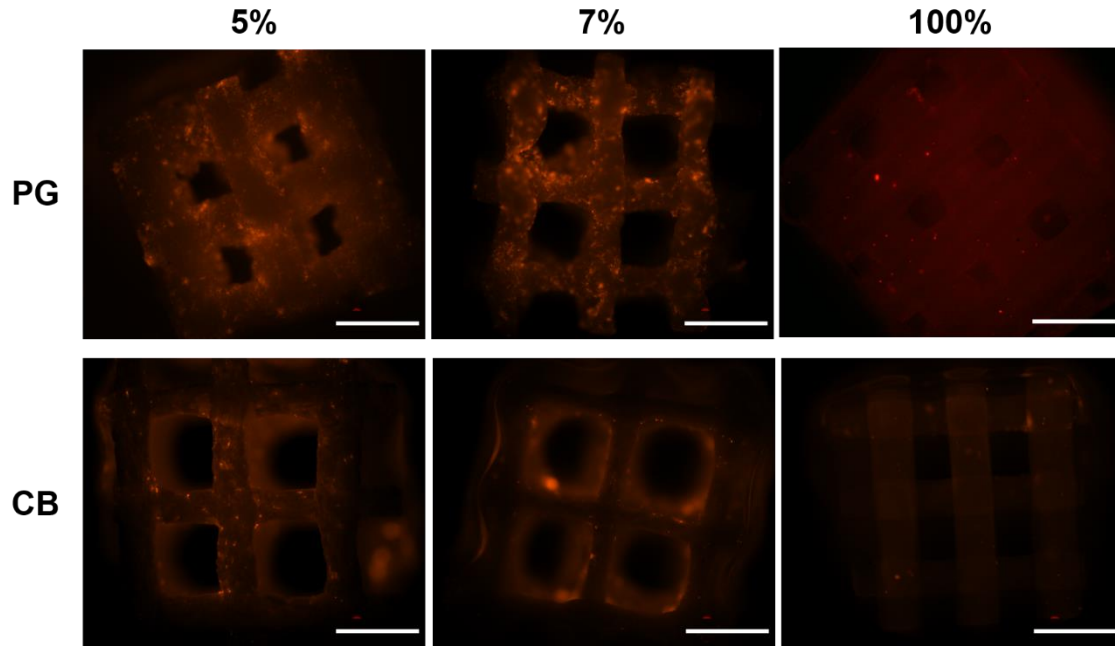


Figure 13 – Immunofluorescence images stained for F-actin of the cells seeded on scaffolds. Scale bar: 1mm.

Ideally, a scaffold implant would not just be tolerated by the cells but induce a specific cell response, e.g. a pro-regenerative phenotype. Therefore, it is relevant to analyse how macrophage shape and polarization is affected by the scaffolds. The morphology of macrophages was evaluated by SEM, where cells presented a distinct shape on the different materials (Figure 14). On 3D-TIPS scaffolds, macrophages presented more filopodia in contrast with macrophages in FDM scaffolds which showed more rounded cells. The differences in morphology are related to the type of migration that macrophages follow, which can be mesenchymal or amoeboid migration (25). The former one is indicated as slow migration with many protrusions, while amoeboid is a fast migration but with rounded cells (25). Recent findings showed that physical properties can stimulate macrophages to alter their phenotype without the addition of soluble factors. This event occurs by the modulation of cell shape where elongated macrophages express anti-inflammatory molecules, like arginase-1, IL-10 and CD206 (21,37). However, the morphology of macrophages could not always indicate a specific action and may be dependent on the source of macrophages. For instance, in a human cell line, THP-1, elongated cells expressed pro-inflammatory cytokines and rounded ones induced an anti-inflammatory phenotype (23,58). Therefore, there is not a

direct correlation yet for morphology and specific phenotype and so the quantification of M1/M2 markers is essential to evaluate the effect on polarization.

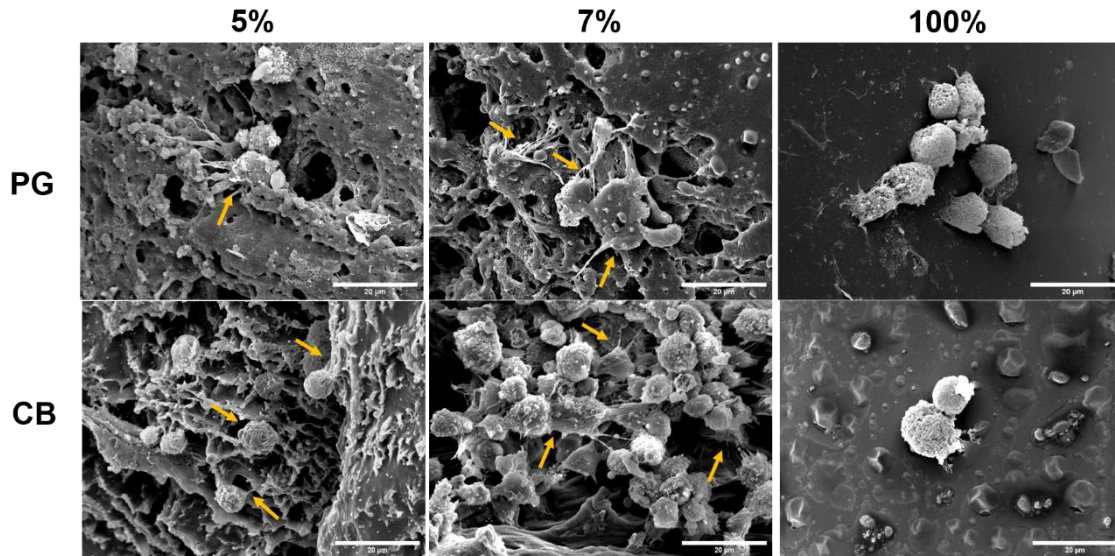


Figure 14 – SEM images representing the changes of macrophage morphology on the different scaffolds. Scale bar: 20μm.

To further evaluate how the phenotype of macrophages is affected by the scaffolds, cells were stained with iNOS and Arginase, and the expression of TNF- α and TGF- β was quantified. Immunofluorescence images (Figure 15) showed that iNOS is the most prevalent marker in all the scaffolds. This tendency was confirmed by cytokine expression, where no detected values of TGF- β were found and higher values of TNF- α were expressed (Figure 16B). Cytokine release quantification proved that CB100 induced a higher release of TNF- α by macrophages (8997 ± 1323 pg/mL), than its porous counterpart CB7. Similarly, macrophages cultured on PG100 also presented a higher release of the same cytokine than porous PG7, suggesting a pro-inflammatory environment on non-porous (FDM) scaffolds. A comparison between materials of similar porosity but different stiffness showed that macrophages cultured on CB100 (material with highest Young's modulus) had the highest release of TNF- α . This could be related to the increased stiffness of this scaffold, compared to the others. It has been shown already that stiffness affects pro-inflammatory cytokine expression when cells are LPS stimulated, showing that softer materials greater suppress pro-inflammatory phenotype (27). However, the effect of stiffness itself is still unclear since there is contradictory data on the effects of stiffness alone. It has been shown that higher stiffness (230kPa) induces increased TNF- α comparing to lower stiffness material (0,3kPa), without LPS stimulation (26). But in another study, macrophages were unresponsive to stiffness alone when comparing 840kPa materials with 130kPa (27). In addition, depending on the cell line used, different responses can happen as seen by the range of TNF- α expression by RAW 264.7 (30–70 pg/ml) and U937 (1250–2750 pg/ml) at stiffness of 0.3–76.8 kPa and BMMs (250–1000 pg/ml) at stiffness of 0.3–230 kPa (22,26). Here, the stiffest material, CB100 ($404,1 \pm 112,5$ kPa), presented the highest expression of TNF- α . CB7, the

second stiffest scaffold, expressed lower values comparing with PG7 and CB100, even if these differences are not statistically significant. Thus, other factors can be affecting TNF- α expression like surface roughness or porosity. Indeed, it was shown by McWhorter et al. that materials presenting certain topographical features not only can release higher amount of pro-regenerative associated cytokines but also decrease iNOS expression (21). Here, the scaffolds from 3D-TIPS technique that are rougher and more porous than FDM scaffolds, showed lower expression of TNF- α suggesting a decrease in pro-inflammatory phenotype.

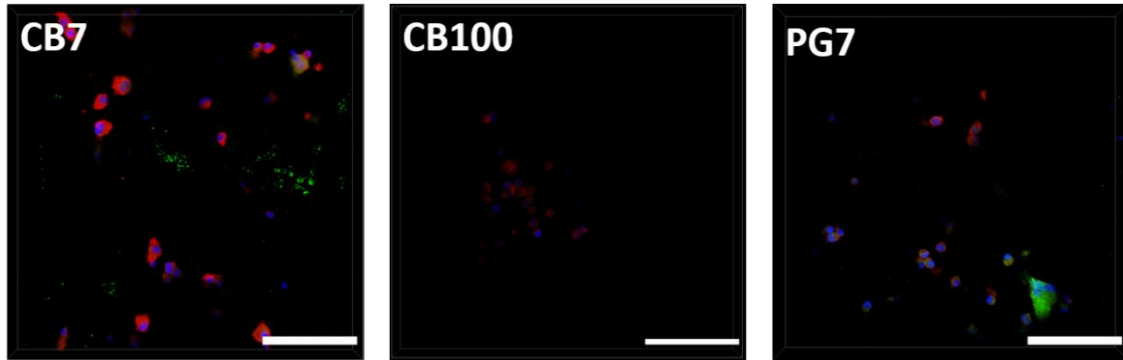


Figure 15 – IF images of macrophages seeded on CB7, CB100 and PG7 scaffolds. The PG100 condition is not shown because of low cell attachment. Scale bar=50 μ m

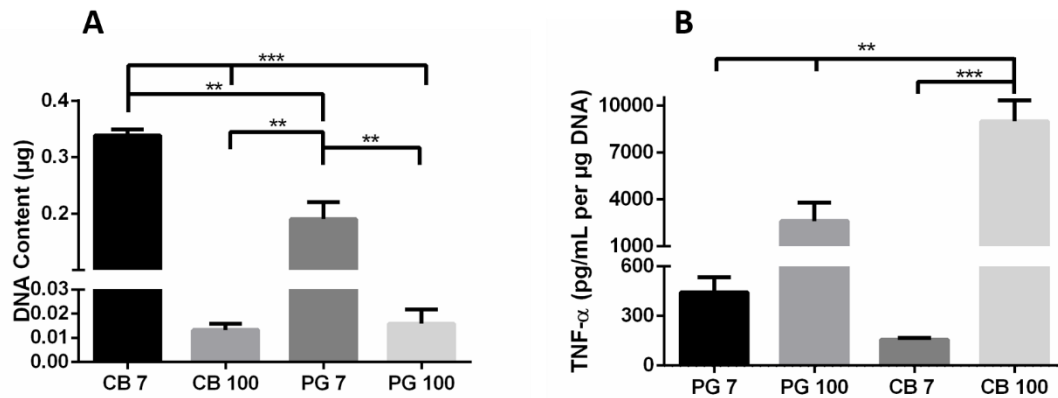


Figure 16 – A: DNA content and B: TNF- α cytokine secretion by macrophages adhered to the scaffolds after 3 days of culture.

The low levels of TGF- β and low expression of arginase can indicate that the scaffolds follow an M1 phenotype, in addition with TNF- α . However, our measurements were performed at 3 days of culture. As the immune response and the states of inflammation progress over time, our results could also imply that cells are still at the beginning of the inflammation cycle, where mostly M1 macrophages are active (4). Therefore, an evaluation of cytokine expression with more time points is suggested to further conclude how these scaffolds affect macrophage function overtime.

3.4. M2 macrophage influence on mesenchymal stem cells (MSCs)

In a regenerative environment guided by a scaffold, various cell types interact with immune cells. Mesenchymal stromal cells (MSCs) are of great interest for tissue repair, not

only for their capacity to differentiate into specific tissues but also for their immunomodulatory properties (59). These cells have been shown to stimulate an anti-inflammatory environment by, for instance, stimulating M2 macrophages. As these cells respond to the factors in the microenvironment, there is a crosstalk between MSCs and macrophages that can influence tissue repair (60).

We mimicked the effect on MSCs in an environment of M2 macrophages polarized by the scaffold. MSCs were cultured using conditioned macrophage media over 10 days and the influence of M2 macrophages on MSC proliferation was evaluated by F-actin and nucleus immunostaining. MSCs adhered to the scaffold and showed viability and proliferation throughout the time of experiment. From the immunostaining results, some conditions suggest a higher proliferation rate on hMSCs cultured with macrophages conditioned media (Figure 17). For instance, 5% CB, 5%PG and 7%CB, on conditioned media showed higher number of cells as compared to MSCs cultured on basal media. From the low magnification images, the cells do not show differences on cell attachment. To confirm the hypothesis proposed that M2 macrophage secretome induced proliferation of MSCs on 3D-TIPS scaffolds, further studies should be conducted. For instance, measurements of the DNA content comparing both conditions would confirm quantitatively if there was a higher proliferation rate. Indeed, if a higher proliferation rate of MSCs cultured on M2 macrophages conditioned media on these scaffolds would be confirmed, this could be a potential focus for localized cell delivery in wound repair. As previously described by others, M2-associated cytokines, like IL-10, VEGF or TGF- β , enhance or maintain the proliferation of MSCs as compared to media without cytokines. This effect was also tested on direct co-cultures with M2 macrophages and higher proliferation rates were also found (58). Therefore, if an anti-inflammatory environment surrounds the scaffold, the MSCs delivery would result on its proliferation and potentially wound healing.

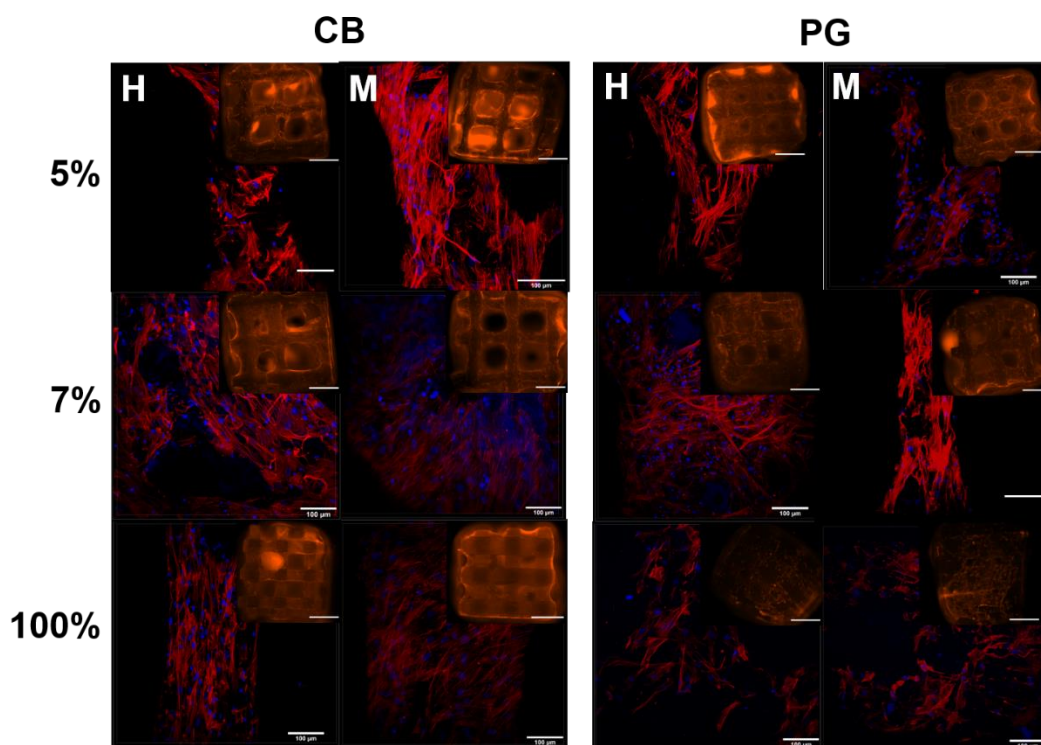


Figure 17 – IF images stained for F-actin (red) and Nuclei (blue) with different scaffolds. Here the H, stands out for basal media hMSCs conditions and M for hMSCs treated with M2-stimulated macrophages secretome Scale=100µm and in upper corner scale= 1mm.

3.5. Support Bath

As seen in the previous results, the scaffolds fabricated by 3D-TIPS technique presented deformed and flattened fibers. This fact interferes on the main advantage of additive manufacturing, controllability, since the scaffold shape is poorly defined. To overcome this limitation, a support bath was proposed for this project. A support bath acts like a Bingham plastic, which means that behaves like an elastic solid at rest but after applying enough stress it flows as viscous fluid (61,62). In addition, after the application of stress, the support bath has the ability to revert its solid state. As such, by the application of a stress by a nozzle, while printing, the support bath should have the capacity to constrain the shape of the material, even if it is liquid. These properties allow printing of soft materials without collapsing and maintaining the shape (62,63).

For this work, two different systems of support baths were tested, an organogel and a hydrogel. The organogel was a lecithin / glycerol / n-decane system and it was chosen since its solvent, n-decane, has a lower freezing point, around -29,7°C(64), comparing to the solvent of the printing gel, 1,4-dioxane that is 12°C (65) and water (0 °C). These properties could allow the printing of the material and then, upon freezing, the recovery of only the frozen scaffolds that would then freeze dried. To find the ratio between lecithin/glycerol/n-decane, various concentrations of each reagent were evaluated by inverted positioning the

vials, assuming jellification when the mixture was not able to flow down. The chosen concentration was 60 % lecithin / 2 % glycerol / 38 % n-decane, since it was the only one that formed a stable gel as (Figure 18), that stayed on top after inverting the vial. Individual fibers were printed in this gel but some drawbacks were noticed while printing. For instance, the bath presented an opaque colour that makes difficult the process of printing and, after the motion of the nozzle, the gel did not return to its original form. After printing, the fibers were removed with a tweezer but the lecithin gel remained in the fibers. As this support bath was mainly constituted to organic solvents it is essential that these reagents would be removed so it would not interfere with the scaffold biocompatibility. Indeed, printing of a full scaffolds should be tested on this support bath and the capability to remove the scaffold as a solid upon freezing should be evaluated. One improvement to this technique would also be to use bleached lecithin since a transparent support bath would allow higher control during the printing process.

The second support bath tested was composed of a gelatin/glycerol/water system and the chosen concentrations to print were from 1,3% to 2,2% of gelatin (w/v) in 10% (v/v) and 90% (v/v) of glycerol and water, respectively. From these concentrations, none of the gels act like a support since the lattice pattern was not formed and the first layer did not attach to the bottom of the petri dish, which increased the difficult for printing layer by layer. In fact, as the stress of the nozzle was applied, all the support bath was affected instead of a localized liquefied part of the material. The main advantage of this gel would be the effortless removal of the scaffold by simply dissolving in water. However, several optimizations would be needed to achieve the ideal rheological properties.

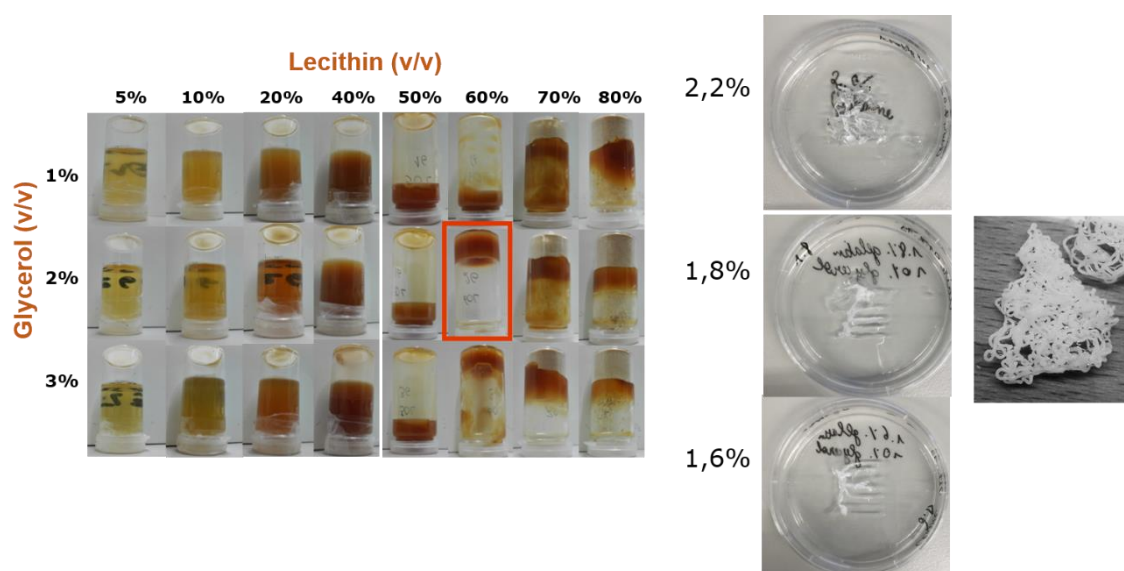


Figure 18 – Photographs for Lecithin gels in the right of the panel and Gelatine in the left.

The main problems of both support baths systems tested were that neither of them maintained the shape and that the printing pattern was not defined. This could mean that the support baths did not act like a Bingham plastic or the stress of the motion of the needle was high. To further continue with these systems of support bath, improvements should be done

like using bleached lecithin, separating the scaffolds from the support bath after freezing and evaluating if the printed scaffolds retain the same or higher porosity. In addition, the rheological properties of the support bath could be measured to study its Bingham plastic behaviour. Recently, granular gels have been tested as support bath showing great results in printing soft materials by a smooth variation between solid state and fluid (66). The main advantage of these gels is that the material does not depend of its rheological properties and so the stress of the nozzle would not change its composition or its properties but only locally, providing precision and stability for printing (66). However, this study failed to show the fabrication of traditional porous scaffolds as the ones studied here, and the potential to maintain porosity on the z-axes of the printed object is still not addressed. Therefore, the lecithin and gelatine here used could also be transformed in microparticles to form a granular gel that support printing and allow to create porosity on the z-axes of the object.

3.6. *In vivo* response to PCLLA scaffolds

To evaluate the influence of the physical properties of 3D-TIPS scaffolds as compared to FDM scaffolds on the immune response *in vivo*, the scaffolds were surgically implanted in subcutaneous pockets of athymic nude rats. Tissue surrounding the scaffolds was excised three or six weeks after material implantation and evaluated by histology (Figure 19). 4 different scaffolds were implanted; CB7, PG 7, CB100 and PG100.

In scaffolds with low mechanical strength, e.g. PG, a dense fibrous capsule was formed mostly in FDM scaffolds, in both time points, as visualized from Masson's trichrome staining. The 3D-TIPS scaffolds of PG showed a thin fibrous capsule after 3 weeks that evolved to a denser capsule after 6 weeks with collagen formation inside the fibers (Figure 19C, D). 3D-TIPS scaffolds also showed higher cellular infiltration, by H&E staining, than FDM scaffolds whereas the porosity was lower. In addition, PG scaffolds showed very deformed scaffolds without any fiber visible for 3D-TIPS and with a rounded structure in FDM scaffolds. The shape of scaffold presented can be related to the degradation of the material. The degradation of PCLLA copolymer leads to the production of lactic acid. The lactic acid is usually degraded by the organism, but if the degradation rate is elevated, the organism can surpass its capacity to metabolize lactic acid. As such, a chronic inflammation might be happening forming the fibrous capsule, as seen in our results. The causation of the fibrous capsule could be confirmed by the staining of M1/M2 macrophages markers, such as, iNOS, IL-1R1, CD 86 for M1 and SRBI/IL, CD206, Arginase-1, CD163 for M2, as others did (34,35,49). The degradation of the polymer can happen by the interaction with media or with the help of macrophages by the formation of FBGC and production of ROS or degradative enzymes (12). H&E staining revealed concentration of cells represented by purple regions around the implant that can be FBGC suggesting a chronic inflammation on these scaffolds. CB scaffolds do not show an evident deformation of the scaffold, maintaining its shape over the implantation period. CB copolymer contains 0 / 100 ratio of D / L lactide enantiomers of PLA in its composition while PG has a ratio of 15 D / L lactide enantiomers. This differences can explain the different degradation rate between scaffolds

since it was reported that the D / L amorphous forms degrade faster than pure L forms that are more crystalline (67).

From CB scaffolds, higher cell infiltration was detected both in 3D-TIPS and FDM scaffolds. In 3D-TIPS scaffolds, cells appeared in the microporosity of the fibers indicating pore interconnectivity. In FDM scaffolds cells infiltrated between the fibers and it is also evident the deposition of collagen. Comparing both conditions, 3D-TIPS scaffolds showed a thinner fibrous capsule around the material, while FDM have more collagen between fibers. This enhances the importance of having z-direction porosity since this can augment the interaction between scaffold and tissue.

Altogether, the scaffolds from amorphous PCLLA (PG) have shown higher degradation and a thicker fibrous capsule. In addition to the degradation factor, the fact that FDM have lower surface roughness can affect collagen deposition by macrophages. As seen previously by others, flat materials showed an extent fibrous capsule comparing it with the ones with 1D wrinkles (35). Furthermore, the size of porous has also an influence in macrophages infiltration and collagen production, where smaller pores (34 μ m) have shown higher cell infiltrate and thinner fibrous capsule than bigger pores (160 μ m) material (34). Here, FDM scaffolds of CB with just macroporosity (500 μ m-800 μ m) showed increased collagen deposition between the fibers while 3D-TIPS scaffolds, with microporosity (5 μ m-100 μ m) showed more cell infiltration and a thin fibrous capsule, correlating with the previous studies.

From these results, it would be also interesting to evaluate macrophage infiltration and function in the collagen formation on the scaffolds. In addition, markers of M1/M2 markers could be stained to compare between the conditions and to evaluate in which locations of the scaffold macrophages differentiation was steered more into M1 or M2 phenotype.

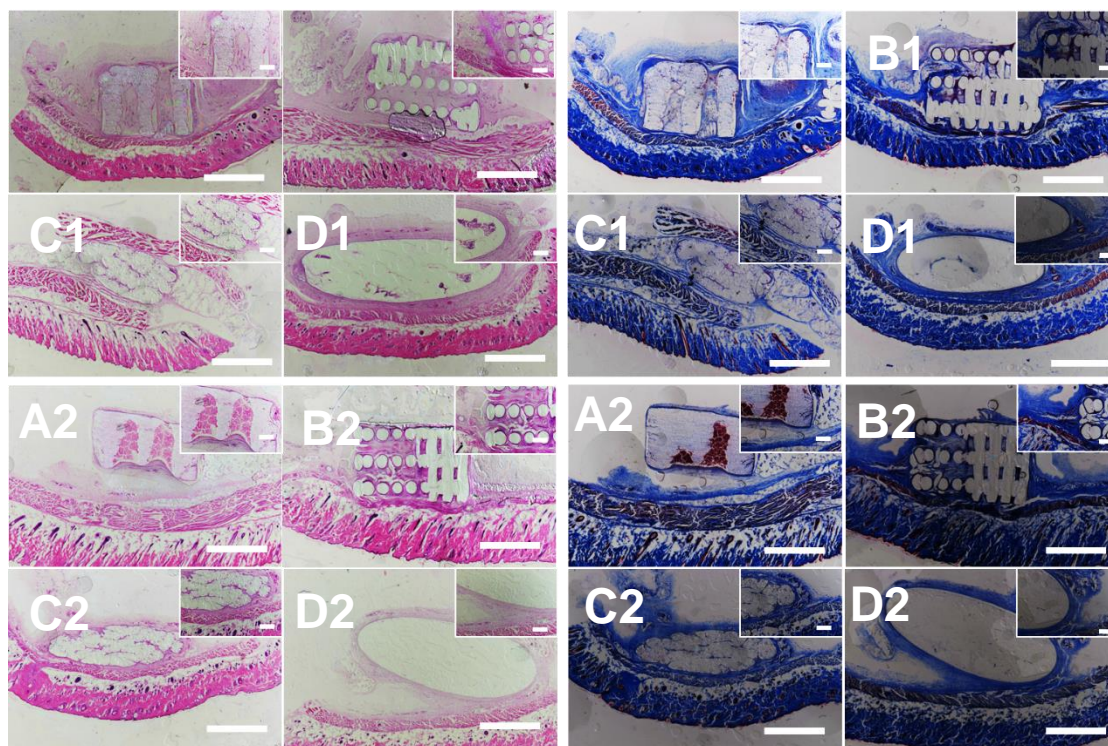


Figure 19 - Cellular infiltration and matrix deposition in scaffolds produced by 3D-TIPS and FDM after subcutaneous implantation for 3 weeks (1) and 6 weeks (2): (Left) tissue integration by Hematoxylin and Eosin (H&E) staining and (Right) collagen production by Masson's trichrome (M&T) staining. A) CB7, B) CB100, C) PG7 and D) PG100 are represented in low magnification (scale = 2000 μ m) and a $\times 4$ magnification (scale = 500 μ m) in the upper corner.

4. Conclusion

The combination of additive manufacturing and TIPS appears to be a great technique to produce scaffolds with tuneable form, porosity and topography depending on the concentration of the polymer. Comparing it with the FDM technique, 3D-TIPS scaffolds presented higher surface roughness and thus higher available surface area to interact with cells, higher porosity and lower Young's modulus materials. These properties have been reported to influence immune response by the interaction with macrophages and so, in this report we aimed to investigate whether 3D-TIPS scaffolds are good candidates for macrophage modulation towards a pro-regenerative phenotype.

In this report, two copolymers of PCLLA with chemical similarities but expected differences in crystallinity and thus, mechanical properties were investigated. Both copolymers showed great potential for 3D-TIPS by consistently maintaining its morphology while printing from polymer organogels with 5% and 7% (w / v) of material and by the microporosity formed within the fibers. The more crystalline copolymer, CB, showed higher stiffness and porosity than the more amorphous one, PG. The surface roughness was higher in 3D-TIPS scaffolds than in FDM ones as well as the porosity. Both copolymers showed biocompatibility and low cytotoxicity levels. Furthermore, on PCLLA films, macrophages were evaluated in terms of their polarization comparing to stimulated M1 or M2 phenotypes. PG showed higher expression of arginase in all conditions and M1 stimulated macrophages expressed greater levels of TNF- α .

From the investigation of how topography and porosity affect macrophages, it was shown that 3D-TIPS scaffolds with higher surface roughness induced more cell adhesion and the formation of more filopodia on the cells than FDM scaffolds. In addition, FDM scaffolds presented the higher values of TNF- α than 3D-TIPS indicating that this technique can reduce the inflammation. Whether 3D-TIPS scaffolds induce an anti-inflammatory phenotype is still not clear since the expression of TGF- β and arginase were low in all the conditions. As such, further studies should be inquired with different M2 markers and evaluating how the cytokine expression is affected over time.

The capacity of 3D-TIPS scaffolds to reduce the inflammation was also shown by in vivo studies, in the amorphous copolymer PG. FDM scaffolds presented a bigger fibrous capsule than the more porous 3D-TIPS scaffold. PG showed higher degradation rate than CB which also increased the fibrous capsule. 3D-TIPS of CB had cell infiltration within fibers confirming the pore interconnectivity but FDM CB scaffolds also showed great capacity for cell infiltration by its porosity on the z-axis.

Indeed, the 3D-TIPS technique could be improved in terms of scaffold shape controlability and to increase the porosity on the z-axis. This could be done by the use of a support bath that acts like a Bingham plastic. In this report, lecithin / glycerol / n-decane system and gelatin / glycerol / water system did not show the preferential properties to improve 3D-TIPS. Therefore, further studies could be done eventually with granular gels that show promising results in other reports.

As these scaffolds are intended for implantation and to stimulate tissue repair by modulation of the immune response, co-culture with other involved cells, like fibroblasts or MSCs is an essential step to understand tissue regeneration. Here, we showed a preliminary study where the secretome of M2 stimulated macrophages appeared to enhance MSCs proliferation. However, further analysis via, i.e., measurement of total DNA would still be required.

The observations throughout this report indicate that the scaffolds with higher roughness and porosity represented by 3D-TIPS scaffolds could be an interesting path to follow in order to reduce acute inflammation and to promote tissue repair while being controllable for its physical properties and morphology.

5. Valorisation

Every biomaterial implantation goes through an immune response that can eventually lead to the encapsulation of the material. Adverse immune reactions to biomaterials can affect tissue healing and quality of life of the patients. Nowadays, an immune responsive implant is being pursued in order to overcome the foreign body reaction and stimulate pro-regenerative environment. Many applications of implants have been addressed, as therapeutic and diagnostic tools for cancer, cardiovascular defects or orthopaedic implants to avoid rejection of transplantations (68). The physical properties of a biomaterial have been an interesting route to modulate immune response, since it would not be necessary complicated delivery systems of cytokines or pharmacological molecules. In this report, the additive manufacturing and TIPS are combined to create scaffolds that ideally mimic the microtopographies of ECM and reduce the acute inflammation while promoting a pro-regenerative environment. With this technique personalized anatomical geometries would be created and augment the open porosity which then enables nutrient diffusion, oxygen transport, waste removal and blood vessel ingrowth in addition to increase cell infiltration. The technique enables the creation of these scaffolds in few steps and the tunability for porosity, surface roughness and mechanical properties depending the polymer used, concentration of polymer and solvent/non-solvent ratio.

6. References

1. Franz S, Rammelt S, Scharnweber D, Simon JC. Immune responses to implants e A review of the implications for the design of immunomodulatory biomaterials. *Biomaterials*. 2011;32:6692–709.
2. Wilson CJ, Clegg RE, Leavesley DI, Pearcy MJ. Mediation of Biomaterial–Cell Interactions by Adsorbed Proteins: A Review. *Tissue Eng* [Internet]. 2005;11(1–2):1–18. Available from: <http://www.liebertonline.com/doi/abs/10.1089/ten.2005.11.1>
3. Anderson JM, Rodriguez A, Chang DT. Foreign body reaction to biomaterials. *Semin Immunol*. 2008;20:86–100.
4. Zhou G, Groth T. Host Responses to Biomaterials and Anti-Inflammatory Design—a Brief Review. *Macromol Biosci*. 2018;18(8):1–15.
5. Vishwakarma A, Bhise NS, Evangelista MB, Rouwkema J, Dokmeci MR, Ghaemmaghami AM, et al. Engineering Immunomodulatory Biomaterials To Tune the Inflammatory Response. *Trends Biotechnol* [Internet]. 2016;34(6):470–82. Available from: <http://dx.doi.org/10.1016/j.tibtech.2016.03.009>
6. McNally AK, MacEwan SR, Anderson JM. α subunit partners to β 1 and β 2 integrins during IL-4-induced foreign body giant cell formation. *J Biomed Mater Res Part A* [Internet]. 2007 Sep 1;82A(3):568–74. Available from: <https://doi.org/10.1002/jbm.a.31161>
7. McNally AK, Jones JA, MacEwan SR, Colton E, Anderson JM. Vitronectin is a critical protein adhesion substrate for IL-4-induced foreign body giant cell formation. *J Biomed Mater Res - Part A*. 2008;86(2):535–43.
8. DeFife KM, Jenney CR, McNally AK, Colton E, Anderson JM. Interleukin-13 induces human monocyte/macrophage fusion and macrophage mannose receptor expression. *J Immunol* [Internet]. 1997;158(7):3385–90. Available from: <http://www.ncbi.nlm.nih.gov/pubmed/9120298>
9. Kao W, McNally A, Hiltner A, Anderson J. Role for interleukin-4 in foreign-body giant cell formation on a poly(etherurethane urea) in vivo. *J Biomed Mater Res*. 1995;29:1267–75.
10. Klopffleisch R. Macrophage reaction against biomaterials in the mouse model – Phenotypes , functions and markers. *Acta Biomater* [Internet]. 2016;43:3–13. Available from: <http://dx.doi.org/10.1016/j.actbio.2016.07.003>
11. Braga TT, Agudelo JSH, Camara NOS. Macrophages during the fibrotic process: M2 as friend and foe. *Front Immunol*. 2015;6:1–8.
12. Klopffleisch R, Jung F. The pathology of the foreign body reaction against biomaterials. *J Biomed Mater Res Part A*. 2017;105A:927–40.
13. Jun J II, Lau LF. Cellular senescence controls fibrosis in wound healing. *Aging (Albany NY)*. 2010;2(9):627–31.
14. Chung L, Maestas DR, Housseau F, Elisseeff JH. Key players in the immune response to biomaterial scaffolds for regenerative medicine. *Adv Drug Deliv Rev*. 2017;114:184–92.
15. Sridharan R, Cameron AR, Kelly DJ, Kearney CJ, O'Brien FJ. Biomaterial based modulation of macrophage polarization: A review and suggested design principles. *Mater Today* [Internet]. 2015;18(6):313–25. Available from: <http://dx.doi.org/10.1016/j.mattod.2015.01.019>
16. Murray PJ, Allen JE, Biswas SK, Fisher EA, Gilroy DW, Goerdt S, et al. Macrophage Activation and Polarization: Nomenclature and Experimental Guidelines. *Immunity* [Internet]. 2014;41(1):14–20. Available from: <http://dx.doi.org/10.1016/j.immuni.2014.06.008>
17. Murray PJ. Macrophage Polarization. *Annu Rev Physiol*. 2017;79(1):541–66.
18. Mosser DM, Edwards JP. Exploring the full spectrum of macrophage activation. *Nat Rev Immunol* [Internet]. 2008;8(12):958–69. Available from:

- <http://www.pubmedcentral.nih.gov/articlerender.fcgi?artid=2724991&tool=pmcentrez&rendertype=abstract>
19. Smith TD, Nagalla RR, Chen EY, Liu WF. Harnessing macrophage plasticity for tissue regeneration ☆. *Adv Drug Deliv Rev* [Internet]. 2017;114:193–205. Available from: <http://dx.doi.org/10.1016/j.addr.2017.04.012>
 20. McWhorter FY, Davis CT, Liu WF. Physical and mechanical regulation of macrophage phenotype and function. *Cell Mol Life Sci*. 2015;72(7):1303–16.
 21. McWhorter FY, Wang T, Nguyen P, Chung T, Liu WF. Modulation of macrophage phenotype by cell shape. *PNAS*. 2013;110.
 22. Patel NR, Bole M, Chen C, Hardin CC, Kho AT, Mih J, et al. Cell Elasticity Determines Macrophage Function. *PLoS One*. 2012;7(9):1–10.
 23. Sridharan R, Cavanagh B, Cameron AR, Kelly DJ, O'Brien FJ. Material stiffness influences the polarization state, function and migration mode of macrophages. *Acta Biomater* [Internet]. 2019;89:47–59. Available from: <https://doi.org/10.1016/j.actbio.2019.02.048>
 24. Adlerz KM, Aranda H, Heather E. Substrate elasticity regulates the behavior of human monocyte - derived macrophages. *Eur Biophys J*. 2016;301–9.
 25. Goethem E Van, Poincloux R, Maridonneau-parini I, Le V. Matrix Architecture Dictates Three-Dimensional Migration Modes of Human Macrophages: Differential Involvement of Proteases and Podosome-Like Structures. *J Immunol*. 2010;184:1049–61.
 26. Previtera ML, Sengupta A. Substrate Stiffness Regulates Proinflammatory Mediator Production through TLR4 Activity in Macrophages. *PLoS One*. 2015;10(12).
 27. Blakney AK, Swartzlander MD, Bryant SJ. The effects of substrate stiffness on the in vitro activation of macrophages and in vivo host response to poly (ethylene glycol) -based hydrogels. *J Biomed Mater Res - Part A*. 2012;100A:1375–86.
 28. Gruber E, Heyward C, Cameron J, Leifer C. Toll-like receptor signaling in macrophages is regulated by extracellular substrate stiffness and Rho-associated coiled-coil kinase (ROCK1/2). *Int Immunol*. 2018;30(6):267–78.
 29. Veiseth O, Dolo JC, Ma M, Vegas AJ, Tam HH, Bader AR, et al. Size- and shape-dependent foreign body immune response to materials implanted in rodents and non-human primates. *Nat Mater*. 2015;14:643–52.
 30. Wang Z, Cui Y, Wang J, Yang X, Wu Y, Wang K. The effect of thick fi bers and large pores of electrospun poly (ε -caprolactone) vascular grafts on macrophage polarization and arterial regeneration. *Biomaterials* [Internet]. 2014;35(22):5700–10. Available from: <http://dx.doi.org/10.1016/j.biomaterials.2014.03.078>
 31. Saino E, Focarete ML, Gualandi C, Emanuele E, Cornaglia AI, Imbriani M, et al. Effect of Electrospun Fiber Diameter and Alignment on Macrophage Activation and Secretion of Proinflammatory Cytokines and Chemokines. *Biomacromolecules*. 2011;12(5):1900–11.
 32. Garg K, Pullen NA, Oskeritzian CA, Ryan JJ, Bowlin GL. Macrophage functional polarization (M1 / M2) in response to varying fi ber and pore dimensions of electrospun scaffolds. *Biomaterials* [Internet]. 2013;34(18):4439–51. Available from: <http://dx.doi.org/10.1016/j.biomaterials.2013.02.065>
 33. Almeida CR, Serra T, Oliveira MI, Planell JA, Barbosa MA, Navarro M. Impact of 3-D printed PLA- and chitosan-based scaffolds on human monocyte / macrophage responses : Unraveling the effect of 3-D structures on inflammation. *Acta Biomater*. 2014;10(2):613–22.
 34. Sussman EM, Halpin MC, Muster J, Moon RT, Ratner BD. Porous Implants Modulate Healing and Induce Shifts in Local Macrophage Polarization in the Foreign Body Reaction. *Ann Biomed Eng*. 2014;42(7):1508–16.

35. Wang T, Luu TU, Chen A, Khine M, Liu WF. Topographical modulation of macrophage phenotype by shrink-film multi-scale wrinkles. *Biomater Sci*. 2016;4:948–52.
36. Chen S, Jones JA, Xu Y, Low H, Anderson JM, Leong KW. Characterization of topographical effects on macrophage behavior in a foreign body response model. *Biomaterials* [Internet]. 2010;31(13):3479–91. Available from: <http://dx.doi.org/10.1016/j.biomaterials.2010.01.074>
37. Luu TU, Gott SC, Woo BWK, Rao MP, Liu WF. Micro- and Nanopatterned Topographical Cues for Regulating Macrophage Cell Shape and Phenotype. *ACS Appl Mater Interfaces*. 2015;7(51):28665–28672.
38. Park SA, Lee SH, Kim WD. Fabrication of porous polycaprolactone/hydroxyapatite (PCL/HA) blend scaffolds using a 3D plotting system for bone tissue engineering. *Bioprocess Biosyst Eng*. 2011;34(4):505–13.
39. Park K, Jung H, Son JS, Park KD, Kim JJ, Ahn KD, et al. Preparation of biodegradable polymer scaffolds with dual pore system for tissue regeneration. *Macromol Symp*. 2007;249–250:145–50.
40. Hollister SJ. Porous scaffold design for tissue engineering. *Nat Mater*. 2006;5(7):590–590.
41. Marascio MGM, Antons J, Pioletti DP, Bourban PE. 3D Printing of Polymers with Hierarchical Continuous Porosity. *Adv Mater Technol*. 2017;2(11):1–7.
42. Di Luca A, de Wijn JR, A. van Blitterswijk C, Camarero-Espinosa S, Moroni L. Tailorable Surface Morphology of 3D Scaffolds by Combining Additive Manufacturing with Thermally Induced Phase Separation. 2017;28(10):2721–31.
43. Visscher LE, Dang HP, Knackstedt MA, Hutmacher DW, Tran PA. 3D printed Polycaprolactone scaffolds with dual macro-microporosity for applications in local delivery of antibiotics. *Mater Sci Eng C* [Internet]. 2018;87:78–89. Available from: <https://doi.org/10.1016/j.msec.2018.02.008>
44. Subia B, Kundu J, Kundu SC. Biomaterial Scaffold Fabrication Techniques for Potential Tissue Engineering Applications. Kundu J, editor. 2010;Ch. 7. Available from: <https://doi.org/10.5772/8581>
45. Akbarzadeh R, Yousefi AM. Effects of processing parameters in thermally induced phase separation technique on porous architecture of scaffolds for bone tissue engineering. *J Biomed Mater Res - Part B Appl Biomater*. 2014;102(6):1304–15.
46. Tanaka T, Eguchi S, Saitoh H, Taniguchi M, Lloyd DR. Microporous foams of polymer blends of poly(L-lactic acid) and poly(ϵ -caprolactone). *Desalination* [Internet]. 2008;234(1–3):175–83. Available from: <http://dx.doi.org/10.1016/j.desal.2007.09.084>
47. Chen J, Tu S, Tsay R. A morphological study of porous polylactide scaffolds prepared by thermally induced phase separation. *J Taiwan Inst Chem Eng*. 2010;41:229–38.
48. Li Y. Techniques for fabrication and construction of three-dimensional scaffolds for tissue engineering. *Int J Nanomedicine* [Internet]. 2013;8:337–50. Available from: [papers3://publication/doi/10.2147/IJN.S38635](https://pubmed.ncbi.nlm.nih.gov/24147147/)
49. Wu L, Virdee J, Maughan E, Darbyshire A, Jell G, Loizidou M, et al. Stiffness memory nanohybrid scaffolds generated by indirect 3D printing for biologically responsive soft implants. *Acta Biomater* [Internet]. 2018;80:188–202. Available from: <https://doi.org/10.1016/j.actbio.2018.09.016>
50. Wu L, Magaz A, Maughan E, Oliver N, Darbyshire A, Loizidou M, et al. Cellular responses to thermoresponsive stiffness memory elastomer nanohybrid scaffolds by 3D-TIPS. *Acta Biomater* [Internet]. 2018;85:157–71. Available from: <https://linkinghub.elsevier.com/retrieve/pii/S174270611830744X>
51. Hashizaki K, Sakanishi Y, Yako S, Tsusaka H, Imai M, Taguchi H, et al. New lecithin organogels from lecithin/polyglycerol/oil systems. *J Oleo Sci*. 2012;61(5):267–75.
52. Park JH, Lee BK, Park SH, Kim MG, Lee JW, Lee HY, et al. Preparation of biodegradable and elastic poly(ϵ -caprolactone-co-lactide) copolymers and evaluation as a localized and sustained drug delivery

- carrier. *Int J Mol Sci.* 2017;18(3):1–15.
53. Hsu SH, Hung KC, Chen CW. Biodegradable polymer scaffolds. *J Mater Chem B.* 2016;4(47):7493–505.
 54. Simões CL, Viana JC, Cunha AM. Mechanical properties of poly(ϵ -caprolactone) and poly(lactic acid) blends. *J Appl Polym Sci.* 2009;112(1):345–52.
 55. Onder OC, Yilgor E, Yilgor I. Fabrication of rigid poly (lactic acid) foams via thermally induced phase separation Fabrication of rigid poly (lactic acid) foams via thermally induced phase separation. 2016;(November).
 56. Veillat V, Spuul P, Daubon T, Egaña I, Framer I, Génot E. Podosomes : Multipurpose organelles ? *Int J Biochem Cell Biol.* 2015;65:52–60.
 57. Rodriguez PC, Ochoa AC, Al-Khami AA. Arginine Metabolism in Myeloid Cells Shapes Innate and Adaptive Immunity. *Front Immunol* [Internet]. 2017;8(February):93. Available from: <http://journal.frontiersin.org/article/10.3389/fimmu.2017.00093/full>
 58. Freytes DO, Kang JW, Marcos-Campos I, Vunjak-Novakovic G. Macrophages modulate the viability and growth of human mesenchymal stem cells. *J Cell Biochem.* 2013;114(1):220–9.
 59. Murphy MB, Moncivais K, Caplan AI. Mesenchymal stem cells : environmentally responsive therapeutics for regenerative medicine. 2013;45(11):e54-16. Available from: <http://dx.doi.org/10.1038/emm.2013.94>
 60. Carty F, Mahon BP, English K. The influence of macrophages on mesenchymal stromal cell therapy: Passive or aggressive agents. *Clin Exp Immunol.* 2017;188(1):1–11.
 61. Hinton TJ, Hudson A, Pusch K, Lee A, Feinberg AW. 3D Printing PDMS Elastomer in a Hydrophilic Support Bath via Freeform Reversible Embedding. *ACS Biomater Sci Eng.* 2016;2(10):1781–6.
 62. Hinton TJ, Jallerat Q, Palchesko RN, Park JH, Grodzicki MS, Shue H-J, et al. Three-dimensional printing of complex biological structures by freeform reversible embedding of suspended hydr(1) Hinton, T. J.; Jallerat, Q.; Palchesko, R. N.; Park, J. H.; Grodzicki, M. S.; Shue, H.-J.; Ramadan, M. H.; Hudson, A. R.; Feinberg, A. W. *Thr. Sci Adv* [Internet]. 2015;1(9):e1500758–e1500758. Available from: <http://advances.sciencemag.org/cgi/doi/10.1126/sciadv.1500758>
 63. Compaan AM, Song K, Huang Y. Gellan Fluid Gel as a Versatile Support Bath Material for Fluid Extrusion Bioprinting. *ACS Appl Mater Interfaces.* 2019;11:5714–26.
 64. National Center for Biotechnology Information. PubChem Compound Database. Decane [Internet]. U.S. National Library of Medicine. [cited 2019 Jun 22]. Available from: <https://pubchem.ncbi.nlm.nih.gov/compound/15600#section=Melting-Point>
 65. ACROS Organics | Fisher Scientific. 1,4-Dioxane, 99+%, extra pure, stabilized, [Internet]. [cited 2019 Jun 22]. Available from: <https://www.fishersci.com/shop/products/1-4-dioxane-99-extra-pure-stabilized-acros-organics-4/AC117110010>
 66. Bhattacharjee T, Zehnder SM, Rowe KG, Jain S, Nixon RM, Sawyer WG, et al. Writing in the granular gel medium. *Sci Adv.* 2015;1(8):e1500655.
 67. Pavia FC, la Carrubba V, Brucato V. Tuning of biodegradation rate of plla scaffolds via blending with PLA. *Int J Mater Form.* 2009;2(SUPPL. 1):713–6.
 68. Taraballi F, Sushnitha M, Tsao C, Bauza G, Liverani C, Shi A, et al. Biomimetic Tissue Engineering: Tuning the Immune and Inflammatory Response to Implantable Biomaterials. *Adv Healthc Mater.* 2018;7(17):1–13.

Supplemental Information

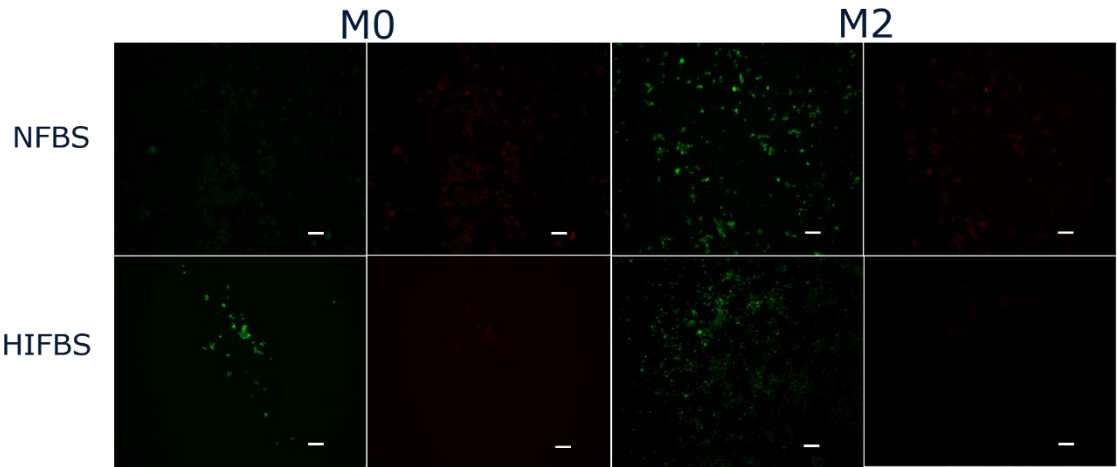


Figure S1 – IF images of macrophages on TCP stimulated for M2 () or non-stimulated (M0) stained for arginase-1 (green) and iNOS (red) in media with Non-Heated FBS (NFBS) and Heat Inactivated FBS (HIFBS), Scale=100μm.

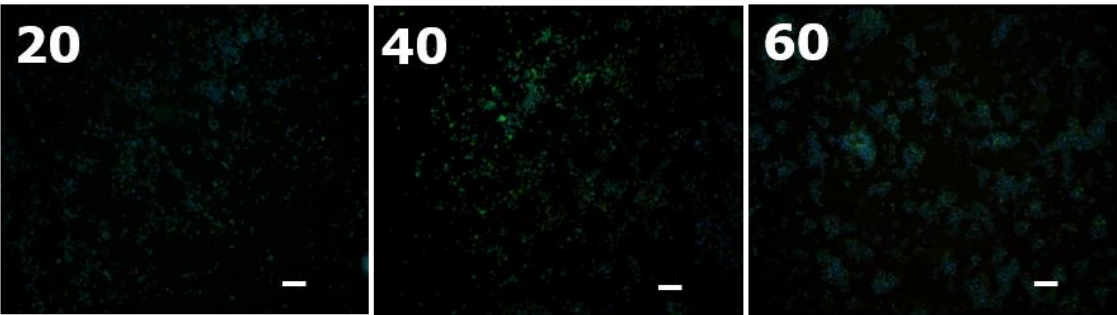


Figure S2 - IF images of macrophages on TCP stimulated for M2 with 20ng/mL, 40ng/mL and 60ng/mL of IL-4/IL-13 stained for arginase-1 (green) and nuclei (blue), Scale=100μm.

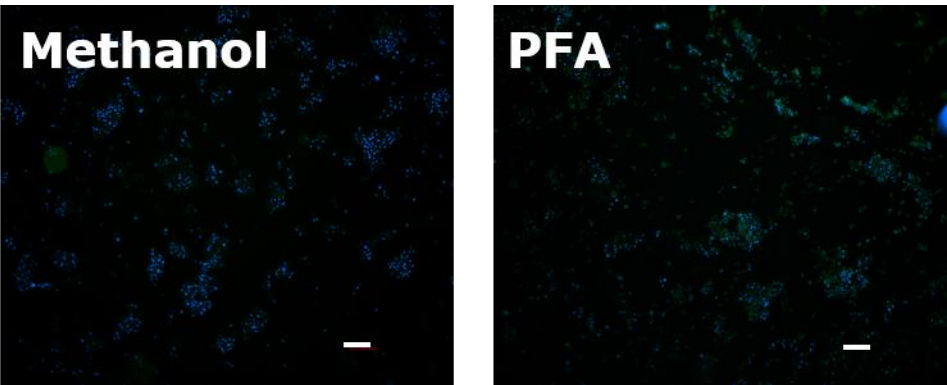


Figure S3 - IF images of macrophages on TCP stimulated for M2 with 20ng/mL of IL-4/IL-13 and two different methods of cell fixation, 100% cold methanol and 4% PFA 13 stained for arginase-1 (green) and nuclei (blue), Scale=100μm.

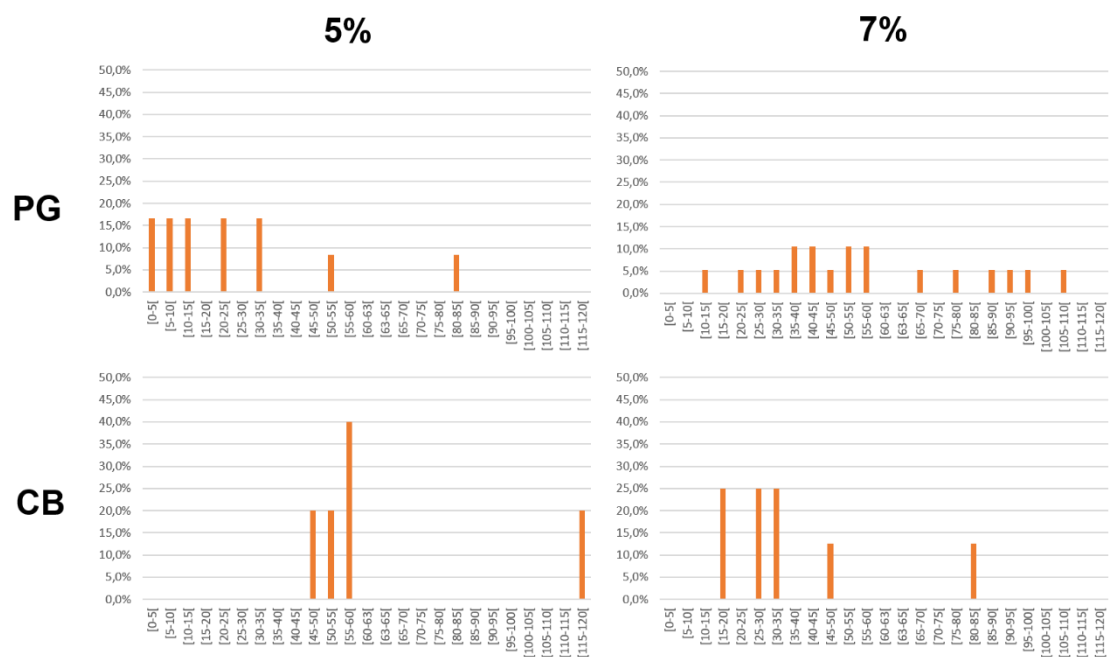


Figure S4 – Relative frequency by the diameter of pores (μm) in 30 pores of CB and PG with 5% or 7% (vol / vol) of PCLLA.